Experimental Analysis of a Three-Photon Entangled State

Diplomarbeit an der Fakultät für Physik
der
Ludwig-Maximilians-Universität München
Arbeitsgruppe Prof. Dr. Harald Weinfurter

Nikolai Kiesel

7. Oktober 2002

Contents

1 Introduction

It is more than 100 years ago that the first step across the border to the quantum world was done. Max Planck studied the blackbody radiation and found an explanation that made him feel extremely uncomfortable – it involved the hypothesis of the quantization of energy. Five years later it was Einstein who made the next step by proposing a return to the particle theory of light which allowed to explain the photoelectric effect.

This was just the beginning of a revolutionary process and in those days it was not foreseeable at all which changes in the world of physics, and even in everydays life would follow. But not new toys like CD-players or digital cameras are the reason why even people from outside the physicists community get more and more interested in quantum physics. Experiments like quantum teleportation [1] and quantum cryptography [2, 3] excite them and trigger the association with futuristic scenarios.

Yet, where are the connections between and where is the transition from the classical to the quantum world. "We cannot, however, do with such old, familiar, and seemingly indispensable terms as "real"..." ([4], Schrödinger in his Nobel lecture in 1933). Quantum mechanics does not fit to the intuition we learn from a (at a first glance) classically appearing world. It was also Schrödinger who introduced the term "Verschränkung" [5] – *Entanglement*, triggered by the paper of Einstein, Podolsky and Rosen (EPR) [6] in 1935, often referred to as the EPR-paradox. In this famous paper, EPR analyze the predictions of a two particle system, where the particles cannot be described independently. Based on the possibility of predicting measurement results of remote particles and, of course, based on locality, i. e. that a measurement on one particle cannot influence the result of a measurement on another one over a large distance, they argued that quantum mechanics cannot be considered complete.

The debate about entanglement and the EPR-paradox was purely philosophical for a long time, and only in 1964 Bell came up with an experimentally testable inequality, that described bounds on the so-called local hidden variable theories (LHV – theories, that should complete quantum mechanics). Bounds that are violated by quantum mechanics [7].

The research on the foundations of quantum mechanics was no more only of theoretical nature. There was an ongoing effort to experimentally violate Bell's

inequality and, even until today, it was not possible to really proof the violation beyond all doubts. The research on possible extensions of quantum mechanics was – and still is – extremely useful to sharpen our intuition on quantum mechanics and the understanding of what entanglement means.

Nowadays the research on entanglement is no more only a research on the foundations of quantum mechanics. The combination of quantum mechanics and information theory proofed to be extremely productive, and applications like quantum cryptography and quantum computation were developed [8]. This, however, does not mean that all of the novel concepts are fully understood. While the entanglement for two spin 1/2 particles (qubits) is well understood, and in the past few years the efforts were focused more and more onto higher dimensional systems and systems consisting out of more particles, it is only two years ago that the entanglement of three qubits has been classified mathematically by Dür.[9].

Experimentally, the development towards higher numbers of entangled particles is an even bigger challenge. It became quite simple to generate entangled pairs of photons. However, only very few experiments achieved entanglement between three and four photons, and only in two experiments with atoms and ions three and four particle entanglement was deduced.

In this work a three-photon entangled state is experimentally analyzed – the W-state (W for Wolfgang Dür who analyzed three particle entanglement in the above mentioned classification). The interest in the W-state arises from the fact, that the entanglement for three particles shows to faces. On the one hand there is the GHZ-state (GHZ for Greenberger, Horne,and Zeilinger who discussed a new kind of violation of predictions of LHV by quantum mechanics for more than two particles) which violates a generalized Bell theorem maximally. On the other hand the entanglement in the W-state (which doesn't show such a strong violation of Bell's theorem) does not completely vanish (in contrast to the GHZ-state) if one out of the three particles is lost. The three-photon entangled GHZ-state has been experimentally realized in 1999 [10], and also the violation of Bell's inequalities for three particles [11] was experimentally approved, but an experimental observation of the W-state was still missing.

The goal of this work therefore was the observation and analysis of the W-state and its characteristic properties. The thesis will begin with a short description of the basic ideas when considering two particles. The concept of qubit and entanglement will be explained and a short introduction of Bell's theorem is given. The following chapter describes the classification of three-qubit states, and the differences between the properties of the W-state and the ones of the GHZ-state. A theoretical description of the scheme for the preparation of the W-state follows in order to explain the basic ideas and the conditions on the experimental realization of the setup. After explaining the actual setup and its alignment the first observation of the W-state is described.

2 Entanglement of two Particles

Contents

A new impulse was given to the discussion about the EPR paradox when Bohm presented a new and simpler version of it. While EPR were discussing momentum and position of two particles, Bohm looked at another degree of freedom – the spin. Two spin 1/2 particles (qubits) are the simplest quantum system to look at, because a von Neumann measurement will give four possible outcomes. The door was open for Bell to formulate his theorem, following EPR's program, that allowed even for experimental tests on whether quantum mechanics is fundamental or an extension of the theory by the so called local hidden variables. In this chapter I will introduce the concept of qubit and entanglement in two-particle systems. The EPR paradox will be presented in the Bohm's formulation. Furthermore Bell's theorem in it's most common form, namely the CHSH[1] inequality, will be presented and its violation by quantum mechanics demonstrated.

2.1 Qubits

Let us first consider an experiment on a classical system with two possible results, for example the tossing of a coin. The two possible outcomes of the measurement are head or tail. The coin is in no other state than head or tail. As a quantum mechanical counterpart one could choose the spin of an electron, a two level atom or the polarization of a photon, which will be our choice. A polarization measurement on a photon can be realized by sending it at a polarizing beam splitter with detectors in each output arm. If a detector, mounted in the transmitted (reflected) output, clicks, horizontal (vertical) polarization is measured. The corresponding states are denoted by $|H\rangle$ and $|V\rangle$. In contrast to the classical example of the coin these are

---

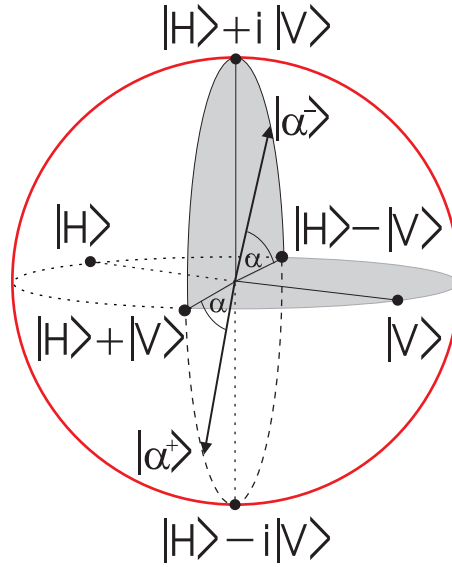[1] Clauser, Horne, Shimony and Holt published the inequlity in [12]

Figure 2.1: The Bloch sphere representation of the Hilbert space of one qubit. The circle with the bold line at the border denotes equally weighted sums of $|H\rangle$ and $|V\rangle$

not the only possible states the photon can have. The superposition principle allows any superposition of the two basis vectors as a state as well. The most general state is $|\psi\rangle = \mu|H\rangle + \nu e^{i\gamma}|V\rangle$ with real parameters μ, ν and γ. In other words, the basis vectors $|H\rangle$ and $|V\rangle$ span a two dimensional Hilbert space H^2. It can be represented by a vector on the so-called Bloch sphere (see fig. 2.1). Such a two-state system is called 'qubit'.

Similar to the state preparation, the projection measurement can be performed in any other basis. One might choose the basis:

$$|\alpha^+\rangle = \frac{1}{\sqrt{2}}(|H\rangle + e^{i\alpha}|V\rangle) \tag{2.1}$$

$$|\alpha^-\rangle = \frac{1}{\sqrt{2}}(|H\rangle - e^{i\alpha}|V\rangle), \tag{2.2}$$

$$\text{where } \langle\alpha^+|\alpha^+\rangle = \langle\alpha^-|\alpha^-\rangle = 1 \tag{2.3}$$

$$\text{and } \langle\alpha^+|\alpha^-\rangle = 0. \tag{2.4}$$

This is a set of basis vectors described by the parameter α. It lies on the great circle of the Bloch-sphere in fig. 2.1[2]. In a consistent way with the definitions made in A.1 the vectors $|\alpha^+\rangle$ and $|\alpha^-\rangle$ are eigenvectors of the observable

$$\sigma_\alpha = \cos(\alpha)\sigma_{\mathrm{x}} + \sin(\alpha)\sigma_{\mathrm{y}} \tag{2.5}$$

---

[2]The circle in the plane orthogonal to the line $|\mathrm{H}\rangle - |\mathrm{V}\rangle$

The probabilities to find a certain measurement outcome in the basis $\{|\alpha^+\rangle, |\alpha^-\rangle\}$ is given by the projection of the state, for example $|L\rangle = \frac{1}{\sqrt{2}}(|H\rangle + i|V\rangle)$, onto the basis:

$$P_+^L(\alpha) = |\langle\alpha^+|L\rangle|^2 = \frac{1}{2}(1 + ie^{i\alpha})(1 - ie^{-i\alpha}) = \frac{1}{2}(1 - \sin(\alpha)), \qquad (2.6)$$

$$P_-^L(\alpha) = |\langle\alpha^-|L\rangle|^2 = \frac{1}{2}(1 - ie^{i\alpha})(1 + ie^{-i\alpha}) = \frac{1}{2}(1 + \sin(\alpha)). \qquad (2.7)$$

The expectation value of the measurement in this basis, i.e. the expectation value of σ_α, is then:

$$\langle\sigma_\alpha\rangle = E^L(\alpha) = P_+^L(\alpha) - P_-^L(\alpha) = -\sin(\alpha). \qquad (2.8)$$

Let us move forward to two-particle systems composed by the particle "A" and "B". Classically, the system might be composed of two coins. There are four possible outcomes of the measurement (head-head, head-tail, tail-head, tail-tail). They correspond to the four possible states of the classical system.

In a system consisting of two qubits there are also four possible outcomes of a measurement (e.g. $|HH\rangle, |HV\rangle, |VH\rangle$ and $|VV\rangle$). But in quantum mechanic the superposition principle allows a two qubit system to be in any superposition of the states corresponding to these outcomes. They are vectors in the Hilbert space $H^2 \otimes H^2$. The joint probabilities for measurement results on two qubits are calculated in the same way as for one qubit – by a projection onto a basis. A possible choice as basis is a combination of the tensor products $|\alpha^i\rangle \otimes |\alpha^j\rangle$ for $i, j\epsilon\{+, -\}$. In this basis the joint probability for a two qubit state $|\psi\rangle$ to be found in $|\alpha_A^+\rangle$ and $|\alpha_B^+\rangle$ is:

$$P_{++}^\psi = |(\langle\alpha_A^+| \otimes \langle\alpha_B^+|)|\psi\rangle| = |\langle\alpha_A^+\alpha_B^+|\psi\rangle| \qquad (2.9)$$

where P_{+-}^ψ, P_{-+}^ψ and P_{--}^ψ are defined in the same way. The measurement outcomes of two particles (A and B) can be correlated. Therefore, we need to define a two particle correlation function:

$$\langle\sigma_{\alpha_A}\sigma_{\alpha_B}\rangle = C_{AB} = P_{++}^\psi - P_{+-}^\psi - P_{-+}^\psi + P_{--}^\psi \qquad (2.10)$$

If the measurements on both qubits always give the same result, then $C_{AB} = 1$; they are perfectly correlated. If $C_{AB} = -1$ they are said to be perfectly anticorrelated and for $C_{AB} = 0$ there is no correlation at all.

2.2 Entanglement

An interesting concept arises if one studies general forms of two-qubit systems. There are pure states that cannot be written as tensor product of states of two single particles,

$$|\psi_2\rangle \neq |\phi_1\rangle \otimes |\phi_1'\rangle, \qquad (2.11)$$

where $|\psi_2\rangle$ is a two-qubit state and $|\phi_1\rangle$ and $|\phi_1'\rangle$ are one-qubit states. $|\psi_2\rangle$ is called an entangled state. An example : $|\psi^-\rangle = \frac{1}{\sqrt{2}}(|HV\rangle - |VH\rangle)$.

Let us calculate the correlations for this measurement results of this state in the basis $\{|\alpha^+\rangle, |\alpha^-\rangle\}$. First we need the four joint probabilities for getting results + and - in joint measurements. For ++ we get

$$P_{++}^{\psi^-}(\alpha_A, \alpha_B) = \frac{1}{2}(e^{i\alpha_B} - e^{i\alpha_A})(e^{-i\alpha_B} - e^{-i\alpha_A}) = 1 - \cos(\alpha_B - \alpha_A). \qquad (2.12)$$

P_{+-}, P_{+-} and P_{+-} are calculated in the same way. Out of these probabilities one obtains with equation 2.10:

$$C(\alpha_A, \alpha_B) = -\cos(\alpha_A - \alpha_B) \qquad (2.13)$$

The two qubits are anticorrelated for any choice of angles where $\alpha_A = \alpha_B$. It is worth mentioning that this is true for the whole Bloch sphere. Only maximally entangled states behave like this. Starting with $|\psi^-\rangle$ one can define a basis for two qubit states out of four maximally entangled states, the so-called Bell-basis.

$$|\phi^+\rangle = \frac{1}{\sqrt{2}}(|HH\rangle + |VV\rangle) \qquad (2.14)$$

$$|\phi^-\rangle = \frac{1}{\sqrt{2}}(|HH\rangle - |VV\rangle) \qquad (2.15)$$

$$|\psi^+\rangle = \frac{1}{\sqrt{2}}(|HV\rangle + |VH\rangle) \qquad (2.16)$$

$$|\psi^-\rangle = \frac{1}{\sqrt{2}}(|HV\rangle - |VH\rangle). \qquad (2.17)$$

Why are these states called *maximally* entangled? A reason for this is explained in the context of the next section.

2.3   The EPR-Paradox and Bell's Theorem

Now we arrive to the point to follow Einstein, Podolsky and Rosen and ask: "Can Quantum Mechanical description of the Physical Reality be Considered Complete?" . In [6] their answer is "NO". They presented an argument based on perfect anticorrelations in momentum and position of two locally separated particles. Bohm offered a new formulation of the gedankenexperiment involving the state $|\psi^-\rangle$ considered before. The heart of the argument, though, was still the same. I want to present only a short outline of the argument here (there's a big amount of literature - to mention just some: [13, 14]) Befor the argument is presented it is necessary to present a term, that EPR introduced: *element of reality*. In their opinion any complete physical theory must have a counterpart to each element of reality, where their definition of elements of reality is [6]:

> *"If, without in any way disturbing a system, we can predict with certainty (i.e., with probability equal to unity) the value of a physical quantity, then there exists an element of physical reality corresponding to this physical quantity."*

If two particles are in the state $|\psi^-\rangle$ and far apart, then assuming *locality* the measurement on one particle cannot influence the outcome of the measurement on the other one. The perfect anticorrelation allows the prediction of the measurement outcome on one qubit for any basis by a previous measurement on the other qubit. Thus, the polarizations (or spin components – but our notation is the one used for the polarizaton of photons) of each photon are elements of reality. But there is no quantum state, that defines all polarizations of one photon. Under the plausible assumption that a *complete* theory includes a counterpart of any element of reality, quantum mechanics cannot be considered complete.

A seemingly promising way to complete quantum mechanics was the assumption of local hidden variables (LHV) to be intrinsic to the particle. These variables include the information on the possible outcome a measurement performed and they are local – this means, that the outcome of a measurement is predefined while the particle do not interact anymore. Because they are hidden we are not able use them for any prediction. Bell was the first to make an experimental approach feasible. He derived an experimentally testable inequality from the statistical predictions of LHV-theories, that was violated by the predictions of quantum mechanics. I rather refer to [7] for the original argument and the deduction of the inequality and rather introduce the most common form of a Bell inequality, the so called CHSH inequality [12]:

$$B(A, a, B, b) := |C(A, B) - C(A, b) - C(a, B) - C(a, b)| \leq 2, \qquad (2.18)$$

where A and a denote two different bases for the measurements on one particle and B and b the bases for the other one. To give a reason, why the upper bound is 2 if the values of the measurement outcome are predefined, there is a simple argument described in [15]. The result of a single measurement on the first qubit in basis A shall be denoted by v_A. The results on the other possible measurements shall be denoted analogous by v_a, v_B, v_b. The possible results are either $+1$ or -1. If a state like ψ^- is chosen, then the result of a measurement in any basis is an element of reality and already predefined. Therefore one can calculate the combination of correlations for an individual system as:

$$v_A v_B - v_A v_b - v_a v_B - v_a v_b =$$
$$v_B(v_A - v_a) - v_b(v_A - v_a) = \pm 2$$

There is no other possible result for each individual pair than $+2$ or -2. For many measurements on many pair the average of these outcomes cannot exceed a modulus of two.

An example will show that $|\psi^-\rangle$ violates the inequality for the right choice of angles. The correlation function for $|\psi^-\rangle$ was given in 2.13, and for the CHSH inequality one finds:

$$B(0°, 45°, 90°, 135°) =$$
$$|\cos(90°) - \cos(135°) - \cos(45°) - \cos(90°)| = 2\sqrt{2} > 2$$

Quantum mechanics predicts, that the state $|\psi^-\rangle$ violates the CHSH inequality! If there is a source, producing this state (and indeed there is more than one), then the LHV-assumption is experimentally testable. All of the four Bell-states violate the CHSH-inequality maximally for the right choice of angle settings. This is one reason, that justifies the denomination maximally entangled.

In principle one can imagine violations of the inequality up to $B = 4$, because the correlations have values between 1 and -1. It is an interesting question, what is the maximal value B can reach for quantum states. Cirel'son showed that the maximal possible violation by a two qubit quantum state is $2\sqrt{2}$ [16]. This bound is called *Cirel'son's bound*. An easier, but less general proof is given in [15].

This chapter introduced the concepts of interest for this work: Entanglement as a consequence of the superposition principle for two (or many) particle systems. Two qubits, as a simple quantum mechanical system suitable for an analysis of entanglement. The EPR-paradox was presented, which was the basis for Bell's analysis of the statistical predictions of local hidden variable theories. A widely used tool for the test of Bell's theorem, the CHSH inequality, was introduced and it's violation demonstrated by means of one of the four Bell-states. The maximum of this violation is given by Cirel'son's bound. We will continue with systems of three entangled qubits.

3 The W-State

Contents

In this chapter I will look at systems of three particles. After looking at two qubit states, this is the logic step to a more complicated system. Indeed we are faced with a bigger variety of possible states. The most commonly used classification of three-qubit entanglement was first done by Dür et al.[9]. In the first section of this chapter I will introduce the ideas and results of this classification. For an analysis it is necessary to find out what the experimental needs are to proof the observation of the W-state[1]. For that purpose the W-state will be compared to the GHZ-state[2] and a mixed state ρ_{fool}. Furthermore the Bell-Theorems for three qubits will be presented. I will describe the ideas that are especially interesting in respect to the W-state. The violation of Bell's theorem is one of the ingredients for quantum communication schemes like quantum cryptography and quantum key distribution. The chapter will be closed by a short overview of possible applications for the W-state.

---

[1] W like *W*olfgang Dür
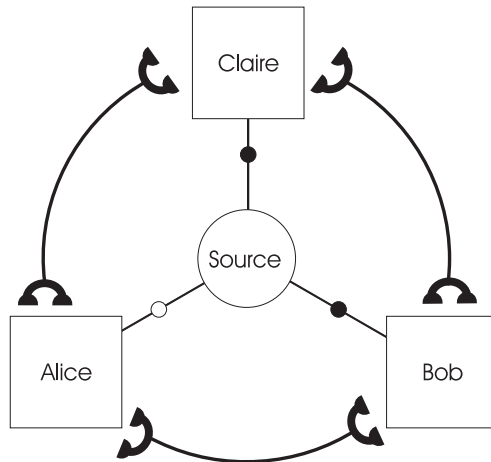[2] for *G*reenberger, *H*orne and *Z*eilinger

Figure 3.1: The three parties get each one particle. They are allowed to do any local operation, but they can only communicate classically with each other, respectivly share no entanglement except for the entanglement in the state itself.

3.1   Classification

Classifications are usually based on giving each particle of the state to spatially separated parties (in our case Alice, Bob and Claire), which are able to do any kind of Local Operations (LO). This includes any operation like measurements and local unitary transformations on their particles and to Communicate Classically with each other (CC). Two states ($|\psi\rangle$ and $|\phi\rangle$) belong to the same equivalence class if under LOCC (local operations and classical communication) Alice, Bob and Claire can transform $|\psi\rangle$ into $|\phi\rangle$ and vice versa,

$$|\psi\rangle \rightleftharpoons |\phi\rangle. \tag{3.1}$$

There are various further rules one can assign to get different classifications [17]. The classification of mixed states has been given in [18]. The case of interest here is the one used by Dür et al. [9] deal with pure states of three particles. Similar to LOCC, each party gets one particle but one does not require that the transformation between the states works every time. It is only necessary that there is at least some probability for Alice, Bob and Claire to transform the state ψ to ϕ. These transformations are called stochastic local operations and classical communication (SLOCC)

The classification leads to six inequivalent classes of three-partite states. They are depicted in fig. 3.2. If a state that belongs to one class is transformable into a
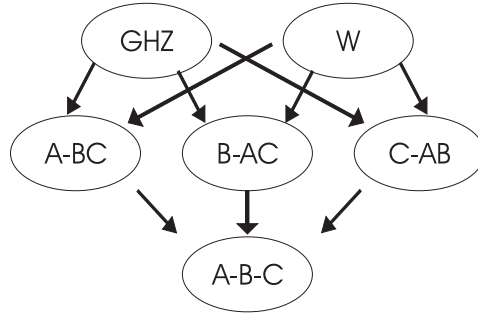
Figure 3.2: The hierarchy of the six inequivalent classes of pure three-partite states. The notation A-BC means that A is a seperable from the system BC, which is entangled (and equally for the other combinations)

state of another class (using SLOCC), then this is indicated by an arrow. One can recognize a hierarchy with the GHZ- and the W-class on the highest level, because no other state can be transformed into a state belonging to these classes. I will give a representative of each of the classes to illustrate the expressions in figure 3.2:

A-B-C : The class of product states being not entangled at all.

$$|\psi\rangle_{A-B-C} = |H\rangle \otimes |H\rangle \otimes |H\rangle \tag{3.2}$$

A-BC : The class of states where two of the qubits are entangled and the third one (here A) is separable from them. (The classes B-AC and C-AB are defined accordingly).

$$|\psi\rangle_{A-BC} = |H\rangle \otimes |\psi^+\rangle = \frac{1}{\sqrt{2}}|H\rangle \otimes (|H\rangle \otimes |V\rangle + |V\rangle \otimes |H\rangle) \tag{3.3}$$

GHZ One class showing real three-partite entanglement. One cannot separate any of the qubits. The representative is the GHZ state[19].

$$|\psi\rangle_{GHZ} = \frac{1}{\sqrt{2}}(|H\rangle \otimes |H\rangle \otimes |H\rangle + |V\rangle \otimes |V\rangle \otimes |V\rangle) \tag{3.4}$$

W The other class showing real three-partite entanglement, though different to the one of the GHZ-class. It is represented by the W-state:

$$|\psi\rangle_W = \frac{1}{\sqrt{3}}(|H\rangle \otimes |H\rangle \otimes |V\rangle + |H\rangle \otimes |V\rangle \otimes |H\rangle + |V\rangle \otimes |H\rangle \otimes |H\rangle) \tag{3.5}$$

To complete this presentation of classifications, I give a coarse reasoning why $|GHZ\rangle$ and $|W\rangle$ belong to different classes. For mathematical detail I refer once more to [9]. Under local unitary (LU)[3] transformations a state can be transformed into different representatives. Each is expressed as a linear combination of a certain number of product terms, e.g. the GHZ-state by $|HHH\rangle$ and $|VVV\rangle$. There is a minimal number of product terms for the representation of each state (e.g. one for product states and two for the states like ψ_{A-BC}). Let us call the minimal number M_{state}. One can show that

- SLOCC-transformations do not change M_{state} for any given state.

- M_W=3 for the W-state and M_{GHZ}=2 for the GHZ-state.

Therefore one cannot transform the W-state to the GHZ-state and vice versa by SLOCC.

3.2   Properties of the W-state

While it is not that surprising that there are differences in the states if none, one or two qubits are separable it is quite astonishing, that there are two classes of real three-partite entanglement! So it will be interesting to see that this is not only a mathematical construction, but that there are measurable differences.

As Dür et al. [9] showed, the W-class states are of measure zero in the set of three qubit states. In other words, the typical three qubit state is a GHZ-class state. In fact, one can always find a GHZ-class state that is almost behaving exactly the same way as any W-class state chosen. For that reason we cannot show experimental differences of the W-state to any arbitrary GHZ-class state, but only to the GHZ-state itself. This way one can learn about the two different kinds of entanglement that can be found when three qubit states are considered.

One is facing another problem, if mixed states are taken into account. A source producing various pure states with certain probabilities (a statistical mixture) can show similar properties as some pure state. It is hard to proof that the experimental data obtained cannot be reproduced this way. In fact, we are not able to prepare a completely pure state (we come to conditions for that in our experiment in 4). Criteria are necessary that allow for tests on the observation of the state. There has been some criticism along these lines on former experiments on the observation of the three photon GHZ-state [20]. It was argued that the experimental data did not proof the observation of the state. In this work I will also not be able to do so. These arguments, however, are not taking into account the source, and I hope that with the knowledge about how the state is prepared there will be few doubt left that the properties observed are the properties of a W-state.

---

[3]LU are part of SLOCC. As one can show LU are equivalent to invertible LOCC

However it is interesting and instructive to compare our state to another one that could theoretically fool us. As it is a mixed state, one needs to use the density matrix formalism:

$$\rho_{\text{fool}} = \frac{1}{3} \left(\rho_{A-BC} + \rho_{B-AC} + \rho_{C-AB} \right) \tag{3.6}$$

Where ρ_{A-BC} denotes the density matrix of the pure state ψ_{A-BC} introduced in the classification above. One can think of a source that emits always an entangled photon pair into two modes and an extra photon in the third mode. The three photons, however, are randomly distributed to the modes.

There is an interesting way to express the W-state, which motivates the choice of the state ρ_{fool}:

$$
\begin{aligned}
\frac{1}{\sqrt{3}} (|\psi_{A-BC}\rangle + |\psi_{B-AC}\rangle + |\psi_{C-AB}\rangle) &= \frac{1}{\sqrt{N}} (\frac{1}{\sqrt{2}} (|H\rangle|H\rangle|V\rangle + |H\rangle|V\rangle|H\rangle) \\
&\quad + \frac{1}{\sqrt{2}} (|H\rangle|H\rangle|V\rangle + |V\rangle|H\rangle|H\rangle) \\
&\quad + \frac{1}{\sqrt{2}} (|H\rangle|V\rangle|H\rangle + |V\rangle|H\rangle|H\rangle)) \\
&= \frac{1}{\sqrt{12}} (2|HHV\rangle + 2|HVH\rangle + 2|VHH\rangle) \\
&= \frac{1}{\sqrt{3}} (|HHV\rangle + |HVH\rangle + |VHH\rangle) \\
&= |W\rangle
\end{aligned}
$$

where $N = \frac{1}{\sqrt{6}}$ is a normalization constant. This means that the W-state is a superposition of the three representatives of the bipartite entangled classes shown in the classification. It is composed out of the same states as the ρ_{fool}, but they are in a superposition in the W-state, whereas they are only classically mixed in ρ_{fool}. In the next section we will see that the two states are giving the same experimental results when all of the photons are measured in the z-basis (which means projection onto the basis vectors $|H\rangle$ and $|V\rangle$; seeA.1).

Loosely spoken one could say that the entanglement of the W-state is mainly intrinsic to the entanglement of the pairs. This is a big difference to the GHZ-state and will be reflected in some properties introduced in this chapter.
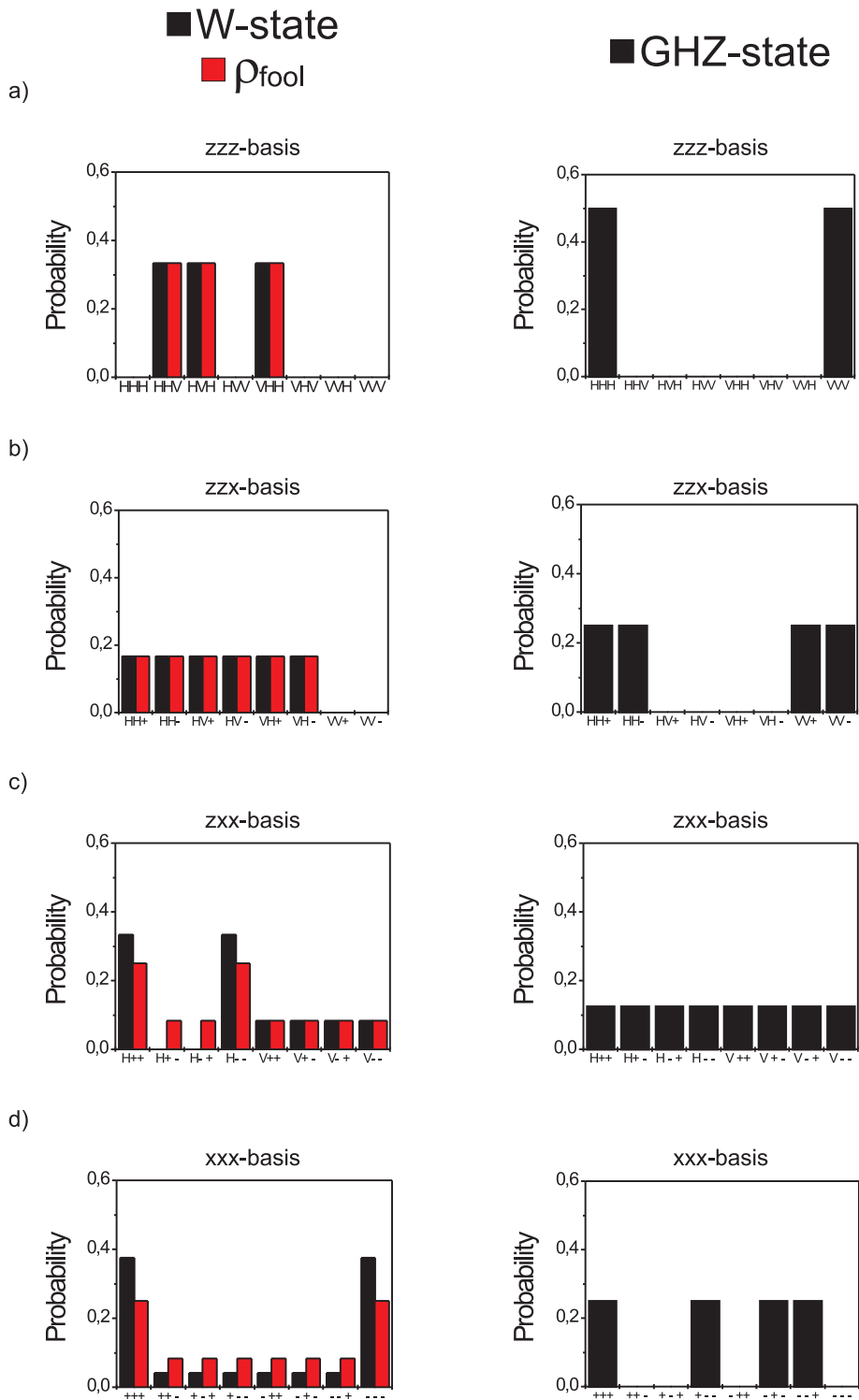
Figure 3.3: On the left the probability distributions in a product basis for the W-state, and ρ_{fool} respectivley are shown. On the right, the corresponding distributions for the GHZ-state are depicted.

3.2.1 Basics

I will use the simplest form of the W-state with equal phases for all three terms. The setup as it is described later on is also producing this state.

$$|W\rangle = \frac{1}{\sqrt{3}}(|HHV\rangle + |HVH\rangle + |VHH\rangle) \tag{3.7}$$

Note that the state is invariant under permutation of the particles. This is also true for the GHZ-state and ρ_{fool}. In fig. 3.3 (page 18) the three states are compared for different basis measurements.

In 3.3.a) it becomes obvious, that it is not enough to look only at the zzz-measurement, (i. e. a measurement of each particle in the z-basis A.1) to proof the observation of a W-state. ρ_{fool} shows the same probability distribution. The W-state shows the characteristic three terms, the GHZ-state two.

In 3.3.b) it is shown, that one still finds the same statistics for ρ_{fool} and the W-state in a zzx-basis measurement.

In 3.3.c), a zxx measurement shows the first differences between ρ_{fool} and the W-state. The W-state has no contributions from $|H+-\rangle$ and $|H-+\rangle$. There is also an interesting feature compared to the GHZ-state. One can at least predict that two terms are missing in case of the W-state, while no prediction can be made in case of the GHZ-state. The opposite is the case in d). In an xxx-basis measurement one can observe every outcome for the W-state (though the contributions are not weighted equally) but not for the GHZ-state. ρ_{fool} shows a slightly different weighting of the terms, but in an experiment the difference would be hard to see.

3.2.2 Measurement of one qubit

Another interesting question is in which state the remaining qubits are left after a readout of a measurement in the third qubit. The following table shows the results for the W- and the GHZ-state:

$$_A\langle V|W\rangle = \frac{1}{\sqrt{3}}|HH\rangle \qquad\qquad _A\langle V|GHZ\rangle = \frac{1}{\sqrt{2}}|VV\rangle$$

$$_A\langle V|W\rangle = \sqrt{\frac{2}{3}}(|HV\rangle + |VH\rangle) = \sqrt{\frac{2}{3}}|\psi^+\rangle \qquad\qquad _A\langle H|GHZ\rangle = \frac{1}{\sqrt{2}}|HH\rangle$$

In the case of the GHZ-state, we have the full information about the remaining two qubits. They are not entangled anymore. This is different for the W-state. Only in 1/3 of the measurements in the z-basis, the result is V and one knows about the other two qubits. If instead the result of the measurement is H, then the other two qubits are maximally entangled. This is a quite distinct difference and gives a handy criterion for an experimental test, because one can analyze the data for the violation of a CHSH-inequality when one particle is in the H-state. We find here an
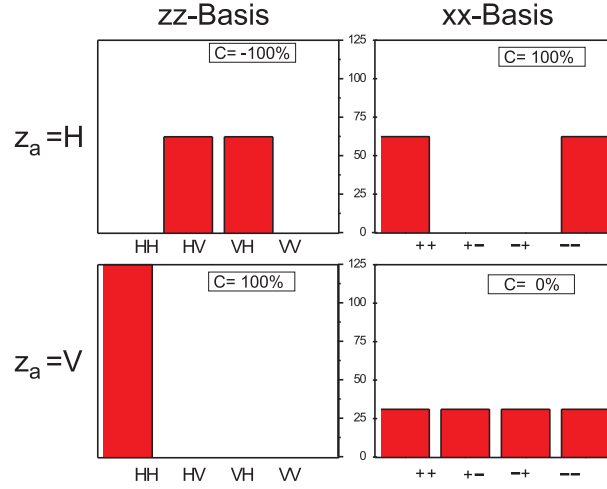
Figure 3.4: The theoretical predictions for the state remaining after one of the particles (e.g. *a*) in the W-state has the measurement outcome $z_a \, \epsilon \{H, V\}$. For z_a=H there are perfect correlations for both, the zz- and the xx- measurement. In case z_a=V there is no correlation between the remaining paricles in the xx-basis measurement at all.

ambivalence: The stronger the correlations are in a state, the lower is its robustness. To show the entanglement in the remaining particles one can take advantage of the fact, that maximally entangled states show full correlations not only for one, but for some bases. We have seen above, that the state of the remaining particles after one is measured in H is $|\psi^+\rangle = (\frac{1}{\sqrt{2}}|HV\rangle + |VH\rangle)$.The basis transformations are A.1:

$$|+\rangle \;\; = \;\; \frac{1}{\sqrt{2}}(|\mathrm{H}\rangle + |\mathrm{V}\rangle)$$

$$|-\rangle \;\; = \;\; \frac{1}{\sqrt{2}}(|\mathrm{H}\rangle - |\mathrm{V}\rangle)$$

Then $|\psi^+\rangle$ can be written in the xx-basis as:

$$|\psi^+\rangle = \frac{1}{\sqrt{2}}(|++\rangle - |--\rangle) \tag{3.8}$$

In the xx-basis the state shows perfect correlation. When considering only pure states, this confirms entanglement. The theoretical predictions for a measurement of this kind is shown in fig. 3.2.2 A more general description of correlations will be subject to the next section.

3.2.3   Correlation functions

Correlation functions in two qubits systems have been introduced in chapter 1. A state is projected onto a general basis which consists of tensor products of basis

vectors $|\alpha_i^+\rangle, \alpha_i^-\rangle$ (where i numbers the particles). For the correlation the sum of the product terms is weighted with the product of the eigenvalues corresponding to the basis vectors. One can write this in compact form:

$$C^{\psi_3}(\alpha_1, \alpha_2, \alpha_3) = \sum_{k_1=\pm 1} \sum_{k_2=\pm 1} \sum_{k_3=\pm 1} k_1 k_2 k_3 |\langle k_1, \alpha_1^{k_1}| \otimes \langle k_2, \alpha_2^{k_2}| \otimes \langle k_3, \alpha_3^{k_3}|\psi_3\rangle|, \quad (3.9)$$

where $k_i \epsilon \{+1, -1\}$. In (2.1) the basis is defined. It is a set of basis vectors on the great circle of Bloch-sphere. The correlation function for the W-state and the GHZ-state are:

$$C^W(\alpha_1, \alpha_2, \alpha_3) = 0 \qquad (3.10)$$
$$C^{GHZ}(\alpha_1, \alpha_2, \alpha_3) = \cos(\alpha_1 + \alpha_2 + \alpha_3) \qquad (3.11)$$

For *any* choice of basis vectors on the great circle of Bloch-sphere the correlation for the W-state is 0, while the GHZ-state shows full correlations. An alternative choice is the equator. We choose as the bases vectors (def. of L/V in A.1):

$$|\phi_i^k\rangle = \frac{1}{\sqrt{2}}(|L\rangle + ke^{i\phi}|R\rangle)$$

The correlation function is calculated similarly:

$$\begin{aligned} C^W(\phi_1, \phi_2, \phi_3) &= -\frac{3}{4}\cos(\phi_1 + \phi_2 + \phi_3) \\ &\quad -\frac{1}{12}(\cos(\phi_1 + \phi_2 - \phi_3) + \cos(\phi_1 - \phi_2 + \phi_3) \\ &\quad + \cos(-\phi_1 + \phi_2 + \phi_3)) \end{aligned}$$

and for the GHZ-state
$$C^{GHZ}(\phi_1, \phi_2, \phi_3) = \cos(\phi_1 + \phi_2 + \phi_3).$$

For the GHZ-state we find the same correlations for the equator as for the great-circle. On the equator the W-state shows also correlations. The correlation functions for $\phi_2 = \phi_3 = 0$ reduce to a cosine for both states.

We can define a theoretical visibility for the correlation function as the "amplitude" of the cosine function. For the GHZ-state when two angles are fixed we still get a visibility of one in the dependence of the correlation on the third angle. If two angles are fixed in the case of the W-state there can also be lower visibilities.

3.2.4 Loss of one particle

With respect to applications it is interesting to find out what happens if one particle is lost, because in any experiment with entangled states particle loss happens. It may be useful if there is still entanglement left in the remaining particles.

Mathematically, this corresponds to tracing out one qubit. In the case of the W-state the result is:

$$\rho_A^W = Tr_A(\rho^W) = \frac{1}{3}|HH\rangle\langle HH| + \frac{2}{3}|\psi^+\rangle\langle\psi^+|$$

and again, we find a state that is entangled. Though, this time, the state doesn't violate the CHSH-inequality anymore. In contrast for the GHZ-state one obtains:

$$\rho_A^{GHZ} = Tr_A(\rho^{GHZ}) = \frac{1}{2}(|HH\rangle\langle HH| + |VV\rangle\langle VV|)$$

For the GHZ-state there is no entanglement anymore. This feature, that the W-state is still having entanglement if one of the photons is lost, is called *entanglement robustness*. It can be shown that the W-state offers the highest amount of residual entanglement of all three-qubit states [9]. This means, that no other state leaves (in average for loss of *any* of the three qubits) that much entanglement in the remaining qubits. What happens with ρ_{fool} if one particle is lost?

$$\rho_A^{\text{fool}} = Tr_A(\rho^{\text{fool}}) = \frac{1}{6}(2|HH\rangle\langle HH| + |HV\rangle\langle HV| + |VH\rangle\langle VH| + 2|\psi^+\rangle\langle\psi^+|) \quad (3.12)$$

Again there is entanglement remaining, but now only in $\frac{1}{3}$ of the cases. It is worth looking at the correlations here: The information we get about the other two qubits is just as little as in the case of the W-state: Only in $\frac{1}{3}$ of the cases we know about the polarization of both left photons. But only in $\frac{1}{3}$ of the cases the remaining photons are really entangled.

In the experimental part of this work the state will be analyzed for entanglement robustness. Usually entanglement is proofed by the violation of Bell-inequalities. As this is not possible for that state, another way has to be found. A secure way to prove its entanglement would be a state tomography [21], and to calculate the Peres-Horodecki criterion [22] out of the deduced density matrix. This criterion provides necessary and sufficient criterion for entanglement.

3.3   W and the Bell Theorem

3.3.1   W's elements of reality

Before certain formulations of Bell's Theorem shall be introduced, which are violated by the W-state, shall be introduced, it will be interesting to ask what are the elements of reality in the W-state [23]. To remember, another time EPR's definition:

> "*If, without in any way disturbing a system, we can predict with certainty (i.e., with probability equal to unity) the value of a physical quantity, then there exists an element of physical reality corresponding to this physical quantity.*"

In the two-particle case elements of reality were identified via the perfect (anti-)correlations, that allow the prediction of a measurement outcome of one particle by a readout of a measurement of the other one. We will have to find out how to obtain information on one of the particles in the three-partite case. For the W-state a first step is to look at its representation in the z-basis:

$$|W\rangle = \frac{1}{\sqrt{3}}(|HHV\rangle + |HVH\rangle + |VHH\rangle) \tag{3.13}$$

If a measurement is performed on two particles in this z-basis, then the outcome of a measurement in z-direction on the third one is perfectly known. If both of the particles are measured to as $|H\rangle$, then the third one is $|V\rangle$ and if they are $|H\rangle$ and $|V\rangle$, the third one is $|H\rangle$. For this reason the outcome of a measurement in the z-basis performed on any of the particles in the W-state is an element of reality. The second step is to look at the W-state in the zxx-basis[4].

$$
\begin{aligned}
|W\rangle \;&= \tfrac{1}{2\sqrt{3}} \;\; (|V++\rangle + |V+-\rangle + |V-+\rangle + |V--\rangle \\
&\qquad\quad +2|H++\rangle - 2|H--\rangle) \\
&= \tfrac{1}{2\sqrt{3}} \;\; (|V\rangle \otimes (|++\rangle + |+-\rangle + |-+\rangle + |--\rangle) \\
&\qquad\quad +2|H\rangle \otimes (|++\rangle - |--\rangle)) \tag{3.14}
\end{aligned}
$$

If the outcome of a measurement on the first particle is H, we can be sure that the outcome of the x-basis measurements on the other two will produce equal results. For this reason an x-basis measurement on the second one gives us full knowledge about the result of an x-basis measurement on the third one without disturbing it in any way.

But what if we had measured V (a situation that occurs in every third measurement)? Then we do not gain any knowledge about possible outcomes of x-basis

---

[4]Though the first particle is chosen to be measured in z-direction, any argument given for one particle is valid for all, because the W-state is invariant under permutation of the particles.

measurements on the remaining to particles. The situation is not as simple as in the two-particle case (2.3), because we cannot be sure whether we get the information about the third particle, but there is a chance to get it. One can, however, continue arguing that it is sure that a measurement on the second instead of the first particle would have had the outcome H, as can be seen by looking at 3.13. But this just means that in principle we could have been lucky enough to choose the other particle for the z-Basis measurement and apply the same argument as before. The conclusion is that the result of an x-basis measurement on a particle of the W-state therefore shold be predefined and thus an element of reality.

But isn't there a problem? If we want to follow the definition of "elements of reality", we should be able to predict the outcome of a measurement in the x-direction on one of the particles. But this is not possible, because we may have bad luck and measure V on the first particle – there will be no chance to find out, what was the value for the x-basis. Thus we cannot know the x-basis value of the third particle.

On the other hand we are arguing from an EPR point of view. This allows us to be sure (as seen in the first step) that the z-basis outcomes are predefined. Then it is just bad luck if the particle we choose for the first measurement is the particle with outcome V. Our luck, however, should not have any impact on the question whether the x-basis measurement outcome of the third particle is an element of reality. It is important that we could have known its value in principle to consider it as a predefined property.

3.3.2 The Mermin Inequality

The CHSH-inequality allows for a test of local realism in the case of two entangled particles as we have seen before. It is an interesting question what possibilities open up for tests on states of more than two qubits. Greenberger, Horne and Zeilinger described in 1989 [19] a gedankenexperiment for a four-qubit GHZ state that allowed for a beautiful new test of local realism. The same argument for a three qubit GHZ-state is presented by Mermin in [24]. Their state allows one to directly apply EPR's argument. By the outcomes of a certain set of measurements (in an ideal experiment) one can conclude the outcome of another one with certainty. But a quantum mechanical calculation of the state predicts that this outcome can never occur. This refutation is "no longer statistical and can be accomplished in a single run" [25]. Yet, for a real experiment it is necessary to formulate an inequality, because one does not get perfect correlations. Mermin derived the inequality for n spin 1/2 particles [25] and proofed its maximum violation by the GHZ-states. I want to present here the three particle case. The inequality reads

$$-2 \leq C(A, B, C) - C(A, b, c) - C(a, B, c) - (a, b, C) \leq 2 \qquad (3.15)$$

where A, a denote two different bases for the first and B, b and C, c two bases for the second and third particle. The maximum violation of this inequality is 4 and is reached by the GHZ-state for $A = B = C = z$ and $a = b = c = x$. This is a much stronger violation, than the one for the CHSH inequality in the two qubit case. The W-state violates the Mermin inequality for $A = B = C = z$ and $a = b = c = x$ with a value of 3. The maximum violation is 3.046 for a more complicated base setting.

3.3.3   A Bell-Theorem without inequalities

In the previous subsection it was demonstrated that the W-state violates the Mermin Inequality, and it's behavior cannot be reproduced by local realistic theories. Still, if one thinks of the GHZ-argument where the test of local realism becomes a test of all or nothing (at least in theory), one longs for a plain logic argument in the case of the W-state, too. Unfortunately a GHZ-type proof of Bell's theorem is not possible for the W-state [15]. Yet, also the W state admits a proof of Bell's theorem without inequalities as Adán Cabello demonstrated in [23]. The argument shall be presented here in the notation used throughout this work.

In quantum mechanics it makes no sense to assign any predefined values to the particles in the W-state. One should keep in mind that the argument is given from the local realistic point of view where we can assign predefined values to the measurement outcomes in the z- *and* x- basis, because they are elements of reality. Then it is possible to select two particles by their polarization (usually they are numbered by their positions a,b and c). The particles i and j are defined to be the ones that have H as measurement result in a z-basis measurement . Then the last particle (k) must have the outcome V. For the W-state it is certain that there are two particles of that kind:

$$P_W(z_i = H \wedge z_j = H) = 1 \tag{3.16}$$

3.14 was used to proof, if the condition that one qubit has a predefined z-value of H, than the outcomes of the other two qubits in a x-basis measurement have to be equal:

$$P_W(x_k = x_j \mid z_i = H) = 1 \tag{3.17}$$
$$P_W(x_k = x_i \mid z_j = H) = 1 \tag{3.18}$$

What are the x-values of the qubits i and j?

Because $z_i = H$ by definition, one can be sure that $x_j = x_k$ because of (3.14). For the same reason also $x_i = x_k$ is true. Then we can be sure that $x_i = x_j = x_k$. This is predicted by local realism, because it allowed us to assume predefined values. What does the quantum mechanical calculation tell us? In the xxx-basis, the state

gets the following form :

$$|W\rangle = \frac{1}{\sqrt{24}} \quad (3|++\rangle - |++-\rangle - |+-+\rangle - |-++\rangle + $$
$$+|--+\rangle + |-+-\rangle + |+--\rangle - 3|---\rangle))$$

The probability to measure x$_i$ =x$_j$ =x$_k$ (which was predicted to be one) is then:

$$P_W(x_i = x_j = x_k) = 2 * (3/\sqrt{24})^2 = \frac{3}{4} = 3/4 \qquad (3.19)$$

Conclusion: If the state is measured in the xxx-basis one has a 1/4 chance to find the x-basis measurement outcomes for the particles as not equal – but this is predicted by local realistic theories. Thus, there is a contradiction between quantum mechanics and local realism in that point.

This is not as beautiful as the GHZ-argument, where one gets an all or nothing test in the last measurement. The difference here is that one has to wait for some time, but as soon as such an event happens the EPR-argument can be refuted.

This result is not yet in an experimentally testable form. By simple algebraic calculations one can deduce an experimentally testable inequality:

$$-1 \leq \quad P(z_i = H \wedge z_j = H) - P(x_k \neq x_j \wedge z_i = H)$$
$$-P(x_k \neq x_i \wedge z_j = H) - P(x_i = x_j = x_k) \quad \leq 0$$

If the values of the W-state are plugged into the inequality, the result is:

$$P_W(z_i = H \wedge z_j = H) - P_W(x_k \neq x_j \wedge z_i = H)$$
$$-P_W(x_k \neq x_i \wedge z_j = H) - P_W(x_i = x_j = x_k) \quad = 0.25 > 0$$

It is worthwhile mentioning that, though the argument fits so nicely to the W-state, the maximum violation provided by the W-state is 0.25, which is the maximum value.

3.3.4   The W-state Violating Cirel'son's Bound

In the first chapter the CHSH-inequality was introduced. And it was argued, that Cirel'son's bound tells us, that two-particle quantum states reach a maximum value of $2\sqrt{2}$. How should two particles out of the W-state violate that bound? Again, one has to recall, that the Bell-inequalities are bounds deduced from a LHV point of view. Let us analyze what happens, when looking for the violation of the CHSH-inequality for two out of the three particles in the W-state. The argument presented here was once more given by Adán Cabello [15]

First, the CHSH-inequality shall be written in a more general form, as the one introduced in the first chapter:

$$|C(A,B) - m * C(A,b) - n * C(a,B) - mn * C(a,b)| \leq 2$$
$$\text{where} \quad m,n \,\epsilon\, \{+1,-1\}$$

These are four CHSH-inequalities for the four possibilities of $\{m, n\}$. The basis chosen now is: $A, B = z$ and $a, b = x$.

The first step is to define, just like in the previous subsection, i and j to label the particles with a z-basis value of H ($z_i = H, z_j = H, z_k = V$). The second step is to select one of the four CHSH-inequalities for each possible value of x_k. (Remember that the state $|+\rangle$ with measurement result $(+)$ has the eigenvalue $\bar{x}_k = +1$ and analogous for $|-\rangle$ – see A.1). The inequality is selected by defining:

$$m := n := -\bar{x}_k \tag{3.20}$$

This is possible because x_k is an element of reality and has a predefined value. The CHSH-inequalities (for both values of $\bar{x}_k$) are:

$$|C(z_i, z_j) + \bar{x}_k * C(z_i, x_j) + \bar{x}_k * C(x_i, z_j) - C(x_i, x_j)| \leq 2 \tag{3.21}$$

Now the different correlations shall be calculated. In [15] one can find different arguments. By definition $\bar{z}_i = \bar{z}_j = +1$ (or different $z_i = z_j = H$):

$$C(\bar{z}_i, \bar{z}_j) = +1 \tag{3.22}$$

It was already previously argued that if one particle is measured in H, then the other two have the same results in an x-basis measurement because in the zxx-basis the W-state is reads 3.14:

$$|W\rangle = \frac{1}{2\sqrt{3}} \quad (|V\rangle \otimes (|++\rangle + |+-\rangle + |-+\rangle + |--\rangle) +$$
$$+2|H\rangle \otimes (|++\rangle - |--\rangle))).$$

Then,

$$C(\bar{z}_i, \bar{x}_j) = C(+1, \bar{x}_j) = C(+1, \bar{x}_k) = \bar{x}_k, \tag{3.23}$$

and

$$C(\bar{x}_i, \bar{z}_j) = C(\bar{x}_i, +1) = C(\bar{x}_k, +1) = \bar{x}_k. \tag{3.24}$$

Finally, from the above, one also learns that if the outcome of a measurement on one particle is V, then the outcomes of measurements in the x-basis on the other two particles is not correlated at all:

$$C(\bar{x}_i, \bar{x}_j) = 0 \tag{3.25}$$

Now it is finally possible to insert the correlations into the inequality:

$$|C(z_i, z_j) + \bar{x}_k * C(z_i, x_j) + \bar{x}_k * C(x_i, z_j) - *C(x_i, x_j)| =$$
$$|1 + \bar{x}_k^2 + \bar{x}_k^2 + 0| = 3 > 2\sqrt{2} \approx 2.83$$

The two particles chosen do not only violate the value of 2 given by local realism - they even violate Cirel'son's bound! In [26], the analysis is done for the GHZ state, which reaches the maximally possible violation of four. The way in which the qubits are labeled, though, is much more natural in the case of the W-state. Again, it is not possible to test this inequality directly, because one cannot know beforehand, which particle is which. If the correlations are expressed in terms of joint probabilities one can deduce an experimentally testable inequality [26]. This inequality is the same as deduced from the argument of Bell's theorem without inequality discussed in the previous subsection (3.20).

$$-1 \leq \quad P(z_i = H \wedge z_j = H) - P(x_k \neq x_j \wedge z_i = H)$$
$$-P(x_k \neq x_i \wedge z_j = H) - P(x_i = x_j = x_k) \quad \leq 0$$

For the violation of Cirel'son's bound it is not enough to exceed 0. Cirel'son's bound for this inequality is:

$$\frac{\sqrt{2} - 1}{2} \approx 0.207 \tag{3.26}$$

3.3.5 Résumé on Bell Theorems

The last subsections have introduced some of the possible tests of local realism that can be done using the W-state. All of them have been introduced for z- and x-basis measurements. A natural question is whether it is possible to a find higher violation for other bases.

The answer is yes and the measurement bases one has to choose are the same for both of the inequalities. A possible choice (expressed in terms ot the corresponding operator as in [23] – see in the appendix A.1 and section 2.1) is:

$$M := A = B = C = \cos(0.628)\sigma_x - \sin(0.628)\sigma_z$$
$$m := a = b = c = \cos(1.154)\sigma_x - \sin(1.154)\sigma_z$$

Expressed in basis vectors, as they have been defined before:

$$|k, M\rangle = \frac{1}{\sqrt{2}}(|L\rangle + k e^{i0.628 + \pi/2}|R\rangle)$$
$$|k, m\rangle = \frac{1}{\sqrt{2}}(|L\rangle + k e^{i1.154 + \pi/2}|R\rangle).$$

The following table shows the necessary and the theoretically achievable violations in all of the three cases:

	W: {x,z}	W: {M,m}	GHZ	LHV	Cirel'son	max. value
Mermin	3	3.046	4	2		4
CHSH	3	3.046	4	2	$2\sqrt{2}$	4
CH-type	0.25	0.262	0.5	0	0.207	.5

Marek Żukowski and his group solved the optimization by using the amoeba numerical procedure [27]. The violation they found corresponds to the one given by Ádan Cabello in [23]. He also found this violation analytically for the angles being distributed in one circle on the Bloch-sphere [28]

This chapter was concerned with the entanglement in three qubit systems. There are two classes of entangled states that earn special interest, because they show entanglement between all of the three particles: The GHZ- and the W-class. A comparison of the W-state with the mixed state ρ_{fool} in different bases showed the necessity to carefully check whether a state is what it seems to be. The features, that make the entanglement in the W-state special have been shown: On the one hand, it's correlations are less strong than the ones in the GHZ-state. The correlation functions proof this. On the other hand the entanglement in the W-state is more robust against a measurement, respectively the loss of one particle. The weaker correlations of the W-state are also reflected by the fact that it does not violate Bell inequalities as strongly as the GHZ-state does. Some Bell theorems that are of special interest for an analysis of the W-state have been shown: The widely used Mermin inequality, a Bell theorem without inequalities for the W-state, and a two particle inequality for two out of the three particles in the W-state which violates the upper bound for the violation by two qubit states.

The still open question how to realize the W-state in an experiment and how to analyze it's properties will be the subject of the next chapter.

4 Design of the Setup

Contents

This chapter intends to introduce all the theoretical concepts necessary for the preparation of the W-state. As a start, the source of the photons shall be described. It is the process of spontaneous parametric down conversion. This method turned out to be reliable in many experiments where two or (more recently) four entangled photons had to be prepared. The next step will be a description of the scheme for the W-state preparation. It shall serve to explain the idea fundamental to the latter realization. A calculation of the setup shall give the basis for minor but helpful changes to the scheme described first. There is not only one way to prepare the W-state. A short overview of possible setups and an extension to W-states for higher numbers of photons shall complete the chapter.

4.1 Spontaneous Parametric Down Conversion

This section will give a short introduction to spontaneous parametric down conversion (SPDC). SPDC has been demonstrated to be an efficient source of entangled photons and was also applied in the present experiment. Let us start the explanation by considering the expansion of the electrical polarization in a crystal:

$$P_i = \epsilon_0 (\chi_{ij}^{(1)} \cdot E_j + \chi_{ijk}^{(2)} \cdot E_j E_j + \ldots) \tag{4.1}$$

Usually this dependence can be approximated linearly, because $\chi_{ijk}^{(2)}$ (and alls higher terms) is small compared to $\chi_{ij}^{(1)}$. But for strong fields and high optical nonlinearities,

one can observe nonlinear processes where $\chi_{ijk}^{(2)}$ is not negligible anymore. In these nonlinear processes the interaction of many waves becomes possible.

Suppose three waves are passing the crystal. A strong one, that will be called the pump beam and two weaker ones, that are usually called idler and signal beam. One observes, that the signal and the idler wave get amplified while the pump wave gets weaker if energy and momentum are conserved:

$$\nu_p = \nu_s + \nu_i \tag{4.2}$$

$$\vec{k}_p = \vec{k}_s + \vec{k}_i \tag{4.3}$$

The conditions look just like conservation of energy and momentum. That effect is called parametric down conversion and is well understood in classical electrodynamics.

The process can also happen spontaneously, that means, a signal and an idler photon are generated out of the pump beam only. This is called *spontaneous parametric down conversion* (SPDC) and cannot be described by classical electrodynamics. It can be interpreted as the decay of a pump beam photon. Photons with the same wavelength, are emitted onto cones. That can be deduced directly from the conditions 4.2 and 4.3. Furthermore, two simultaneously created photons are strongly correlated in energy and momentum. One distinguishes between two types of SPDC:

Type I: The pump beam is extraordinary polarized inside a uniaxial crystal, while the signal and idler photon are ordinary polarized.

Type II: The pump beam is also extraordinary polarized, but one of the created photons is ordinary and the other one extraordinary polarized. This is remarkable, because except for their correlation in energy and momentum they are now strongly correlated in their polarization [29].
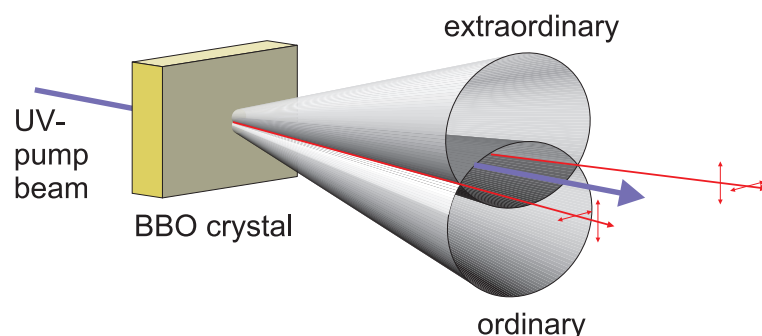

Figure 4.1: The emission cones of the degenerate type II down conversion emission

If the conversion photons have the same wavelength, the process is called *degenerate down conversion*. In our experiment degenerate type II SPDC was applied. When the optical axis of the crystal is tilted the emission cones for the photons are shifted with respect to each others (fig. 4.1). This is due to the different indices of refraction for the orthogonal polarizations in the crystal. In the figure 4.1 degenerate type II down conversion is shown. The upper cone shows the possible emission directions for the extraordinary polarized photon and the lower one the emission of the corresponding ordinary polarized one. On the crossing lines, however, it is not possible to decide to what cone a photon belongs, and therefore one cannot predict the polarization. It is only sure that if one photon is emitted in one of the crossing modes, then the other photon is emitted in the other crossing and that the polarizations of the photons are orthogonal. For this reason one obtains polarization entangled photons if the modes in the crossing of the two cones are selected. The entangled state obtained is [29]:

$$|\psi^+\rangle = \frac{1}{\sqrt{2}}(|HV\rangle + |VH\rangle) \tag{4.4}$$

If a pulsed pump beam is applied, then the emissions can only take place during the short period when the pulses pass the crystal. The general form from which the case of multiple emission events can be deduced is[29]:

$$Z \cdot e^{-ic(a_V^\dagger b_H^\dagger + a_H^\dagger b_V^\dagger)}|0\rangle \tag{4.5}$$

where Z is a normalization constant, c is proportional to the pump intensity and $a_V^\dagger, b_H^\dagger, a_H^\dagger$ and $b_V^\dagger$ represent the photon creation operators. By expansion we obtain [30]:

$$Z \cdot (c(a_V^\dagger b_H^\dagger + a_H^\dagger b_V^\dagger) + \frac{c^2}{2}(a_V^\dagger b_H^\dagger + a_H^\dagger b_V^\dagger)^2 + ...)|0\rangle \tag{4.6}$$

The first term gives the state $|\psi^+\rangle$ shown before. The second term is responsible for the four-photon emission we are interested in. It's expansion

$$a_V^{\dagger\,2} b_H^{\dagger\,2} + a_H^{\dagger\,2} b_V^{\dagger\,2} + 2a_V^\dagger b_H^\dagger a_H^\dagger b_V^\dagger \tag{4.7}$$

results in the following superposition of photon number states:

$$|2H_a, 2V_b\rangle + |2V_a, 2H_b\rangle + |1H_a, 1V_a, 1H_b, 1V_b\rangle \tag{4.8}$$

One finds with equal probability each:

- Two H-polarized photons in a and two V-polarized ones in b

- Two V-polarized photons in b and two H-polarized ones in a

- H- and a V-polarized photon in both arms, a and b

It is remarkable that the weighting for all the terms in equation (4.8) is equal. This is not what one would expect from an emission of two pairs, where the probability for emission of different photons into one mode would be 1/2. Equal amplitudes occur due to an interference effect. If the two pump photon decays were distinguishable by time of arrival of the photon pairs at the detectors, then the equation (4.8) would not be valid. How is this indistinguishability achieved? In the experiment presented here ultrashort pulses (130 fs) pump the down conversion crystal. The coherence time (the temporal uncertainty) of the photons collected from the down conversin process – given by bandwidth of the applied filter – is much larger than the time uncertainty of creation of the two photons. Thus one cannot distinguish by time of arrival, to which pair the photon belonged.

4.2 Two-Photon Interference

In fig. 4.2 the W-setup is shown. The following section will describe it in more detail. I just want fo focus on the fact, that two photons are overlapped on BS_1, which causes an interference effect, which plays an important role for the design of the setup.

Two modes m and n are overlapped on a symmetric beam splitter. The transformation performed on a symmetric beam splitter can be described as [31]:

$$m^\dagger \quad \rightarrow \quad \frac{1}{\sqrt{2}}(m^\dagger + i \cdot n^\dagger) \tag{4.9}$$

$$n^\dagger \quad \rightarrow \quad \frac{1}{\sqrt{2}}(n^\dagger + i \cdot m^\dagger) \tag{4.10}$$

where $m^\dagger$ and $n^\dagger$ are creation operators in mode m and n.

Two distinguishable photons are incident on the beam splitter in both input modes:

$$m^\dagger \cdot n^\dagger \quad \rightarrow \quad \frac{1}{2}(m^\dagger + i \cdot n^\dagger)(n'^\dagger + i \cdot m'^\dagger) \tag{4.11}$$

$$\tag{4.12}$$

where the primed operators express the distinguishability. In a photon number state description this becomes:

$$\frac{1}{2}(m^\dagger + i \cdot n^\dagger)(n'^\dagger + i \cdot m'^\dagger)|0\rangle = \frac{1}{2}(i|mm'\rangle + |mn'\rangle - |nm'\rangle + i|nn'\rangle) \tag{4.13}$$

There is 1/2 probability for the photons to split up and 1/4 to find both in the mode m, respectively mode n. If they are indistinguishable we obtain out from (4.11)(neglecting the global phase):

$$\frac{1}{\sqrt{2}} \cdot (m^{\dagger^2} + n^{\dagger^2}) \tag{4.14}$$

and as photon number state:

$$(m^{\dagger 2} + n^{\dagger 2})|0\rangle = \frac{1}{\sqrt{2}}(|2\rangle_m + |2\rangle_n) \tag{4.15}$$

The photons never split up. The probability to detect two photons in one mode is 1/2 for each mode and therefore double compared to the case of distinguishable photons.

What means indistinguishability? There are certain factors, that could make the photons distinguishable. The time of arrival at the detector (temporal or longitudinal coherence), the mode if the overlap is not perfect (transversal spatial coherence), their color (spectral coherence) and their polarization.

It is not possible to temporally distinguish two photons if they are detected within their coherence time. The coherence time of a photon corresponds to a longitudinal extension of the photon (the spacelike uncertainty). For a gaussian wave packet this is just the inverse of the bandwidth. If the delay between the photons is varied, then one can observe the transition between distinguishability and indistinguishabability in a dip in the coincidence rate between the output modes for zero delay. The effect was experimentally verified by Hong, Ou and Mandel (HOM-dip)[32]. They found the following relation for the coincidence count rate behind a recombining beam splitter.

$$N_c = C(T^2 + R^2)\left(1 - \frac{2RT}{R^2 + T^2}e^{-(\Delta\omega\,\delta\tau)^2}\right) \tag{4.16}$$

where C is the coincidence count rate far outside the dip, R and T are reflection and transmission coefficient of the beam splitter, $\Delta\omega$ is the bandwidth of the detected photons and $\delta\tau * c$ is the path length differnce.
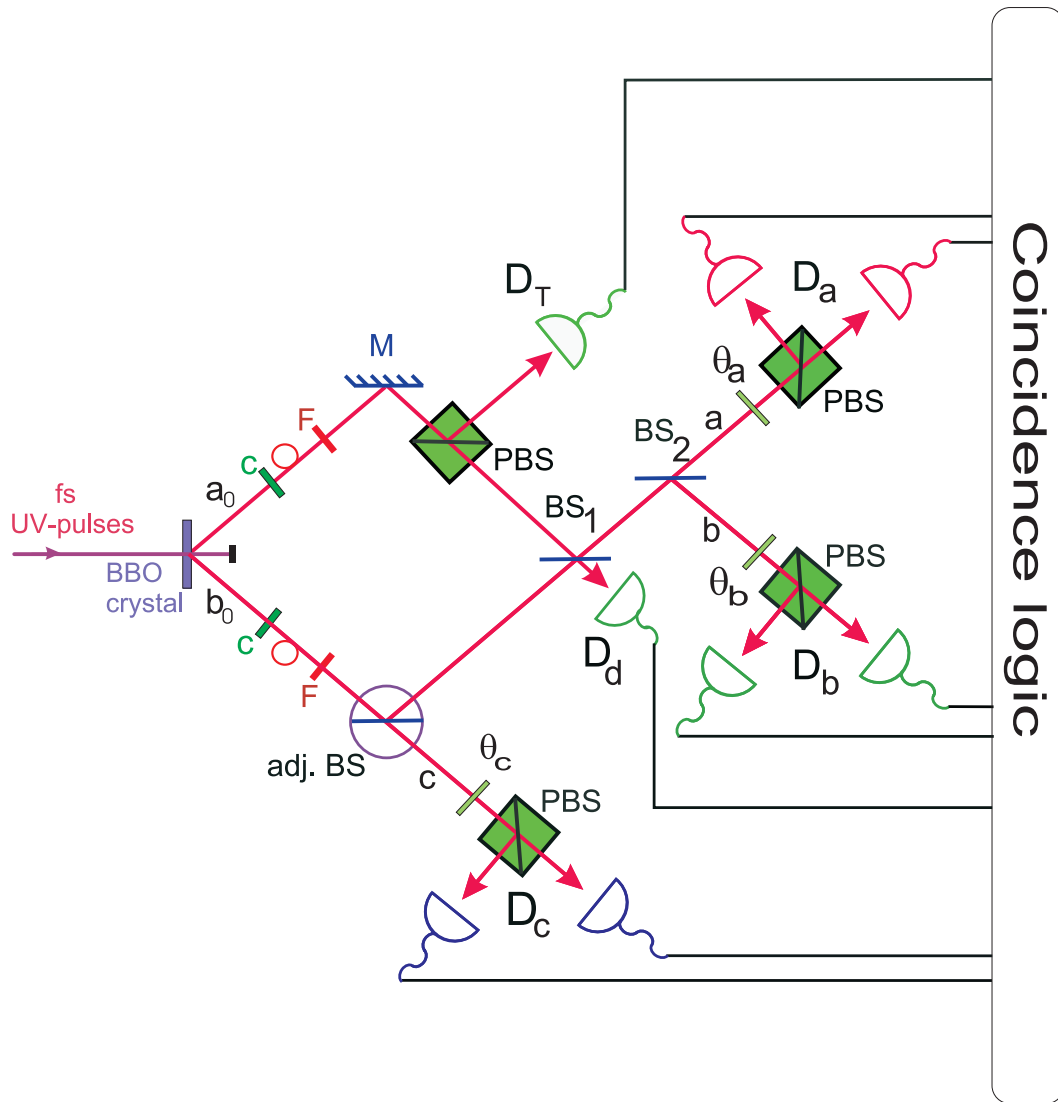
Figure 4.2: Experimental setup for the demonstration of the entangled three-photon W-state where C, F, M, BS, adj. BS and PBS stand for compensator cristal, filter, mirror, non-polarizing beam splitter, adjusting beam splitter with a reflection coefficient $R_V = 2R_H$ and polarizing beam splitter. Three polarization analyzers with wave plates set to $(\theta_i(i = a, b, c))$ are used.

4.3   The Principle

In this section the scheme of the W-state preparation setup (4.2) will be explained. It should make plausible, how the setup allows to observe the W-state out of four photons created in the process of spontaneous type II parametric down conversion (4.1). The four photons enter the setup at I_{a_0} and I_{b_0} after the polarization of the photons in mode b_0 is transformed (H→V and V→H). The modes are split up either via the polarizing beam splitter PBS_{trig} (with output modes t and a_0) or the adj. BS (with output modes b'$_0$ and c). The modes a_0 and b'$_0$ are overlapped at BS_1 and only one of the output modes is used for the state preparation. This mode is split by BS_2 which has the output modes b and c. The W-state is then found in a,b and c.

   The main idea behind the preparation of three-photon entanglement out of SPDC is the so-called *post-selection*. It was already used in previous experiments, like in the observation of the three-photon entangled GHZ-state [10]. Post-selection means, that only events where a photon is detected in each of the four output modes of the state preparation are selected for the analysis. This ensures that processes, where only one pair of photons is created by the source are not counted. Further, only those cases where the photons in a_0 split up at PBS_{trig} and the ones in mode b_0 at adj. BS contribute, since otherwise there is no way to distribute the four photons to the modes t,a,b and c.

   The photon that enters mode t is vertically polarized (V-polarized) due to PBS_{trig} and doesn't contribute to the W-state, but serves as a trigger for the post selection. Its companion in b_0 has, due to the transformation in the fiber the same polarization (V-polarization).
The one in the transmitted output mode of PBS_{trig} is H-polarized and its companion in b_0 as well. All together there are three photons left to prepare the state: Two are H-polarized and one is V-polarized – this is what we need for the W-state.

   The photons split up randomly at the adj. BS (the probabilities are given by the splitting ratio). The one in the reflected output is then overlapped with the photon from a_0. The events were both photons are distributed randomly to b and c via the symmetric beam splitter BS_2 are selected. Thus, the V-polarized photon of mode b_0 can go to any of the modes a,b and c and the remaining H-polarized photons are in the other modes. Fig. 4.3 shows all the possibilities and illustrates, that all three terms contributing to the W-state are realized.

   The question arises, why the intermediate step of combining the photons at BS_1 and splitting them up at BS_2 is chosen instead of using the two outputs of BS_1. To obtain a superposition of the three terms $|HHV\rangle$,$|HVH\rangle$ and $|VHH\rangle$ the photons have to overlap such, that there is no way to distingiuish between the possibilities (except for a polarization measurement). If the photons at BS_1 are equally polarized (resp. if H is reflected at the adj. BS) then the situation of section 4.2 occurs and they do not split up. Thus, no coincidence of H-polarized photons in the outputs of
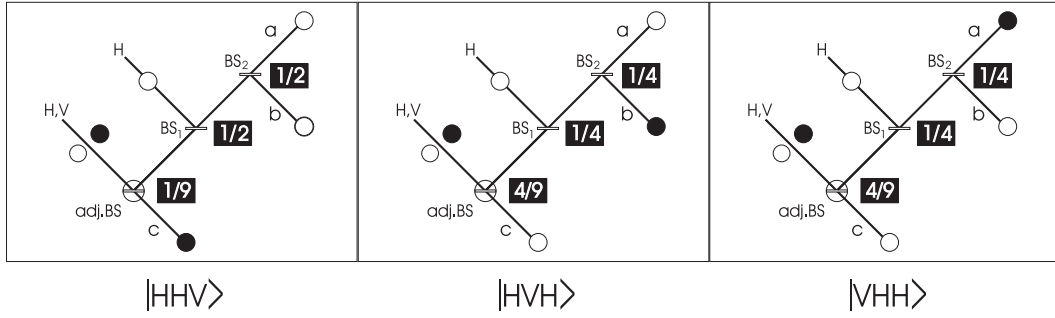
Figure 4.3: The three possibilities for the distribution of the photons with their probabilities

BS_1 will occur.

To obtain the W-state it is not only necessary to prepare a state with $|HHV\rangle, |HVH\rangle$ and $|VHH\rangle$ in superposition, the terms should also have equal amplitudes (i.e. the same probability to be measured). This is achieved by adjusting the adjustable beam splitter to the right splitting ratio. The general condition on the adj.BS is derived in the next section. Fig. 4.3 shows the probabilities for the events at the beam splitters that lead to the different contributions for the choice 1/3 transmission(reflection) and 2/3 reflection(transmission) for vertical (horizontal) polarization at the adj.BS.

4.4 The Calculation

In the last section it became clear that the setup should produce the W-state out of the four-photon state obtained in the second order process of the spontaneous parametric down conversion. A calculation shall complete the analysis of the setup and will show that one is not restricted to an adj. beam splitter with the 1:2 splitting ratio for both polarizations, but that the splitting condition can be somewhat relaxed.

We start with the state produced in the second order process of the down conversion (4.7):

$$\frac{1}{2\sqrt{3}} \left(a_{0_H}^{\dagger 2} b_{0_V}^{\dagger 2} + a_{0_V}^{\dagger 2} b_{0_H}^{\dagger 2} + 2\, a_{0_V}^{\dagger} b_{0_H}^{\dagger} a_{0_H}^{\dagger} b_{0_V}^{\dagger} \right) |0\rangle$$

with the rotation of the polarization in the fiber we obtain:

$$\frac{1}{2\sqrt{3}} \left(a_{0_H}^{\dagger 2} b_{0_H}^{\dagger 2} + a_{0_V}^{\dagger 2} b_{0_V}^{\dagger 2} + 2\, a_{0_V}^{\dagger} b_{0_H}^{\dagger} a_{0_H}^{\dagger} b_{0_V}^{\dagger} \right) |0\rangle.$$

The polarizing beam splitter acts as:

$$a_{0_H}^{\dagger} \rightarrow a_{0_H}^{\dagger}$$
$$a_{0_V}^{\dagger} \rightarrow i\, a_{0_V}'^{\dagger}$$

and transforms the state to

$$\frac{1}{2\sqrt{3}}\left(a_{0_H}^{\dagger 2} b_{0_H}^{\dagger 2} - a_{0_V}^{\prime \dagger 2} b_{0_V}^{\dagger 2} + i\, 2\, a_{0_V}^{\dagger} b_{0_H}^{\dagger} a_{0_H}^{\dagger} b_{0_V}^{\dagger} \right)|0\rangle .$$

We obtain (when only terms where the photons are split are taken into account)

$$i\frac{2}{2\sqrt{3}}\left(a_{0_V}^{\prime \dagger} b_{0_H}^{\dagger} a_{0_H}^{\dagger} b_{0_V}^{\dagger} \right)|0\rangle .$$

The adj. beam splitter transformations are:

$$b_{0_H}^{\dagger} \rightarrow \left(t_H\, c_H^{\dagger} + i\, r_H\, b_{0_H}^{\prime \dagger} \right)$$

$$b_{0_V}^{\dagger} \rightarrow \left(t_V\, c_V^{\dagger} + i\, r_V\, b_{0_V}^{\prime \dagger} \right)$$

with $r_i^2 + t_i^2 = 1$ ($i \epsilon \{H, V\}$) where t_H, t_V, r_H, r_V are the amplitudes for transmission/reflection for horizontal and vertical polarization. The resulting state is:

$$\frac{i}{\sqrt{3}}\, a_{0_V}^{\prime \dagger}\, a_{0_H}^{\dagger} \left(t_H\, c_H^{\dagger} + i r_H\, b_{0_H}^{\prime \dagger} \right)\left(t_V\, c_V^{\dagger} + i r_V\, b_{0_V}^{\prime \dagger} \right)|0\rangle .$$

We neglect contributions of all the terms with 2 photons in one mode and obtain

$$\frac{-1}{\sqrt{3}}\left(t_V r_H\, a_{0_V}^{\prime \dagger}\, a_{0_H}^{\dagger}\, b_{0_H}^{\prime \dagger}\, c_V^{\dagger} + t_H r_V\, a_{0_V}^{\prime \dagger}\, a_{0_H}^{\dagger}\, b_{0_V}^{\prime \dagger}\, c_H^{\dagger} \right)|0\rangle .$$

The next optical component is the overlap beam splitter BS_1 (splitting ratio 50:50):

$$a_{0_H}^{\dagger} \rightarrow \frac{1}{\sqrt{2}}\left(a_{0_H}^{\dagger} + i\, b_{0_H}^{\prime \dagger} \right)$$

$$a_{0_V}^{\dagger} \rightarrow \frac{1}{\sqrt{2}}\left(a_{0_V}^{\dagger} + i\, b_{0_V}^{\prime \dagger} \right)$$

$$b_{0_H}^{\prime \dagger} \rightarrow \frac{1}{\sqrt{2}}\left(i\, a_{0_H}^{\dagger} + b_{0_H}^{\prime \dagger} \right)$$

$$b_{0_V}^{\prime \dagger} \rightarrow \frac{1}{\sqrt{2}}\left(i\, a_{0_V}^{\dagger} + b_{0_V}^{\prime \dagger} \right)$$

We obtain as operator

$$\frac{-1}{2\sqrt{3}}\, a_{0_V}^{\prime \dagger}\left[\; t_V r_H \left(a_{0_H}^{\dagger} + i\, b_{0_H}^{\prime \dagger} \right)\left(i\, a_{0_H}^{\dagger} + b_{0_H}^{\prime \dagger} \right) c_V^{\dagger} + \right.$$

$$\left. + t_H r_V \left(a_{0_H}^{\dagger} + i\, b_{0_H}^{\prime \dagger} \right)\left(i\, a_{0_V}^{\dagger} + b_{0_V}^{\prime \dagger} \right) c_H^{\dagger} \; \right] =$$

$$= \; \frac{-1}{2\sqrt{3}}\, a_{0_V}^{\prime \dagger}\left[\; t_V r_H \left(i\, a_{0_H}^{\dagger 2} + i\, b_{0_H}^{\prime \dagger 2} \right) c_V^{\dagger} + \right.$$

$$\left. + t_H r_V \left(i\, a_{0_H}^{\dagger}\, a_{0_V}^{\dagger} + a_{0_H}^{\dagger}\, b_{0_V}^{\prime \dagger} - b_{0_H}^{\dagger}\, a_{0_V}^{\dagger} + i\, b_{0_H}^{\dagger}\, b_{0_V}^{\dagger} \right) c_H^{\dagger} \right]$$

and select the cases with creation of both photons in a_0:

$$\frac{-i\,a_{0_{\mathrm{V}}}^{\prime\dagger}}{2\sqrt{3}}\left(t_{\mathrm{V}}r_{\mathrm{H}}\,i\,a_{0_{\mathrm{H}}}^{\dagger 2}\,c_{\mathrm{V}}^{\dagger} + t_{\mathrm{H}}r_{\mathrm{V}}\,i\,a_{0_{\mathrm{H}}}^{\dagger}\,a_{0_{\mathrm{V}}}^{\dagger}\,c_{\mathrm{H}}^{\dagger}\right)$$

The transformation at BS$_2$ is:

$$a_{0_{\mathrm{H}}}^{\dagger} \to \frac{1}{\sqrt{2}}\left(a_{\mathrm{H}}^{\dagger} + i\,b_{\mathrm{H}}^{\dagger}\right)$$

$$a_{0_{\mathrm{V}}}^{\dagger} \to \frac{1}{\sqrt{2}}\left(a_{\mathrm{V}}^{\dagger} + i\,b_{\mathrm{V}}^{\dagger}\right)$$

and results in the state

$$\frac{-i}{4\sqrt{3}}\,a_{\mathrm{V}}^{\prime\dagger}\left[\; t_{\mathrm{V}}r_{\mathrm{H}}\left(a_{\mathrm{H}}^{\dagger} + i\,b_{\mathrm{H}}^{\dagger}\right)\left(a_{\mathrm{H}}^{\dagger} + i\,b_{\mathrm{H}}^{\dagger}\right)c_{\mathrm{V}}^{\dagger} + \right.$$

$$\left. + t_{\mathrm{H}}r_{\mathrm{V}}\left(a_{\mathrm{H}}^{\dagger} + i\,b_{\mathrm{H}}^{\dagger}\right)\left(a_{\mathrm{V}}^{\dagger} + i\,b_{\mathrm{V}}^{\dagger}\right)c_{\mathrm{H}}^{\dagger}\;\right]|0\rangle.$$

The contributions where the photons are found in four different modes are:

$$\frac{1}{4\sqrt{3}}\,a_{\mathrm{V}}^{\prime\dagger}\left[\; 2t_{\mathrm{V}}r_{\mathrm{H}}\,a_{\mathrm{H}}^{\dagger}\,b_{\mathrm{H}}^{\dagger}\,c_{\mathrm{V}}^{\dagger} + \right.$$

$$\left. + t_{\mathrm{H}}r_{\mathrm{V}}\left(a_{\mathrm{H}}^{\dagger}\,b_{\mathrm{V}}^{\dagger}\,c_{\mathrm{H}}^{\dagger} + a_{\mathrm{V}}^{\dagger}\,b_{\mathrm{H}}^{\dagger}\,c_{\mathrm{H}}^{\dagger}\right)\;\right]|0\rangle$$

This is expressed as a photon number state:

$$\frac{1}{4\sqrt{3}}\left(2t_{\mathrm{V}}r_{\mathrm{H}}\,a_{\mathrm{V}}^{\prime\dagger}\,a_{\mathrm{H}}^{\dagger}\,b_{\mathrm{H}}^{\dagger}\,c_{\mathrm{V}}^{\dagger} + t_{\mathrm{H}}r_{\mathrm{V}}\,a_{\mathrm{V}}^{\prime\dagger}\,a_{\mathrm{H}}^{\dagger}\,b_{\mathrm{V}}^{\dagger}\,c_{\mathrm{H}}^{\dagger} + t_{\mathrm{V}}r_{\mathrm{V}}\,a_{\mathrm{V}}^{\prime\dagger}\,a_{\mathrm{V}}^{\dagger}\,b_{\mathrm{H}}^{\dagger}\,c_{\mathrm{H}}^{\dagger}\right)|0\rangle =$$

$$= \frac{1}{4\sqrt{3}}|\mathrm{V}\rangle_{\mathrm{trig}} \otimes \left(2t_{\mathrm{V}}r_{\mathrm{H}}|\mathrm{HHV}\rangle_{abc} + t_{\mathrm{H}}r_{\mathrm{V}}|\mathrm{HVH}\rangle_{abc} + t_{\mathrm{H}}r_{\mathrm{V}}|\mathrm{VHH}\rangle_{abc}\right)$$

The condition to obtain equal weight for the three contributions is:

$$2t_{\mathrm{V}}r_{\mathrm{H}} = t_{\mathrm{H}}r_{\mathrm{V}}$$

$$\boxed{\frac{t_{\mathrm{H}}r_{\mathrm{V}}}{t_{\mathrm{V}}r_{\mathrm{H}}} = 2} \tag{4.17}$$

This is the condition for the adjustable beam splitter.

The other information, that we obtain from this calculation is the probability to get a contribution to the W-state out of a second order process, because we started

from a normalized state. The probalitity is given by the norm of the resulting state. For simplicity we assume $t_\mathrm{V} = r_\mathrm{H} = \sqrt{\frac{1}{3}}$ and $t_\mathrm{H} = r_\mathrm{V} = \sqrt{\frac{2}{3}}$ and obtain a probability of:

$$P(W) = \frac{1}{36} \tag{4.18}$$

4.5   Other Ways of Preparation

Very recently, several publications on the subject of W-state preparation appeared. Schemes to produce a W-state of three and four atoms can be found in [33] and [34]. However, one has to face less experimental difficulties in the experimental realization with photons. In [35] Zou et al. present a scheme with linear optical elements to produce a polarization entangled three- or four photon W-state. But the scheme appears rather complicated. During the measurements on our setup, reference [36] appeared suggesting a scheme how to produce a path entangled W-state with one photon and further a multi photon polarization entangled W-state using fiber tritters and single photon sources. Zou et al. presented another scheme applying two EPR-sources the day after. However, the best of these recent publications on the W-state, was presented by Yamamoto, et al. [37]. In their scheme, the W-state is prepared using collinear spontaneous parametric down conversion as source. Their proposal offers a big advantage in comparison to the one that is subject of this thesis. No overlap is needed. Furthermore, the efficiency of the setup is slightly better. While in the presented setup 1/36 of the four-photon processes leads to a W-state (with the possibility to obtain 2/36 when feeding also the photons from output b'$_0$ of BS$_1$ into the free input of BS$_2$) in their setup the ratio is 3/36. A realization of this setup is planned.

This chapter was concerned with the theoretical background of the W-state preparation. The source of entangled photons was described and the state that is the starting point of the setup was presented. A short description of the idea behind the scheme was shown and the probability for observing the W-state was calculated. Further, the calculation showed a necessary condition on the adjustable beam splitter to prepare the state with the right (equal) coefficients.

5 The State Preparation

Contents

The goal of this chapter is to describe the experimental details for the realization of the W-state. The crucial parts of the setup are the adjustable beam splitter and the overlap of two photons on a symmetric beam splitter. Thus they play a central role in the design of the setup.

The setup will be described in the first section. A description of the source of entangled photons, the main components and the detection of the photons follows. Preliminary tests on the fiber coupling and the adjustable beam splitter are included there. The next section describes the stepwise construction of the setup. The overlap at BS_1 (fig. 5.1) allows the observation of a second order interference effect, the so-called Hong-Ou-Mandel dip (HOM-dip), which was also explained in 4.2. The chapter will finish with the analysis of the HOM-dip, which was not only an exciting result, but also an important tool for the alignment.
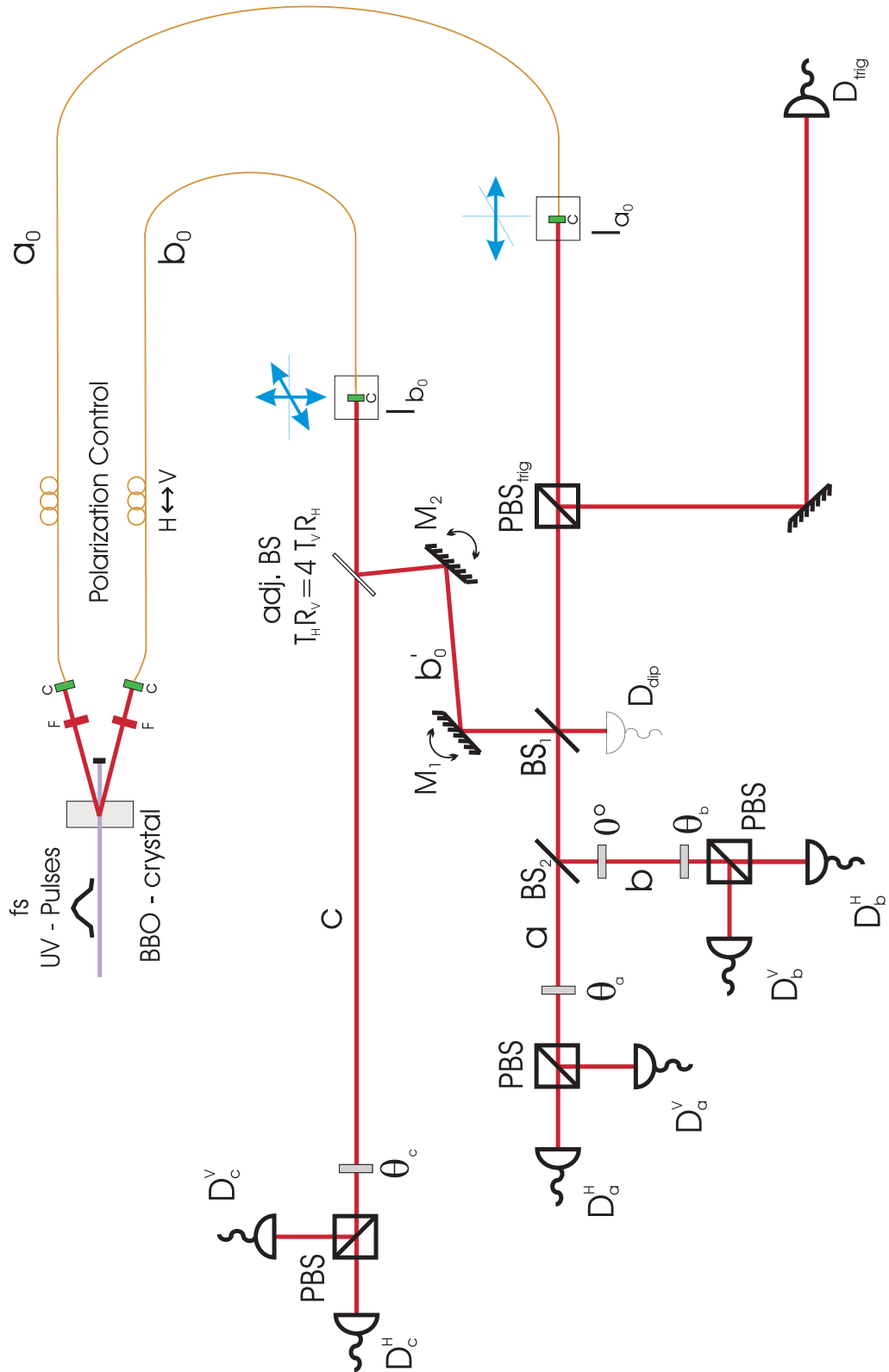
Figure 5.1: Overview of the experimental setup used for the preparation of the Three-Photon Entangled W-state

5.1 Overview

Let us start with the description of the setup as it can be seen in fig. 5.1. A UV-pumped down conversion crystal generates entangled photons in the modes a_0 and b_0. They pass filters (F) and are coupled into single mode fibers. Both of the fibers are equipped with polarization controllers.

The photons from emission mode a_0 are coupled out of the fiber at I_{a_0}. The fiber coupler is mounted onto a translation stage, that is moveable in direction of the photon path. In PBS_{trig} vertically polarized photons get reflected and, after passing another mirror, detected in D_{trig}. Horizontally polarized photons are transmitted and overlapped with photons that were created in b_0.

The mode of the photons emitted in b_0 are coupled out at I_{b_0}. The coupling system allows transversal alignment of the coupling position and the direction. The uncoupled mode b_0 goes then on to the adj. BS. The transmission mode of the adjustable beam splitter (adj. BS) is called c and is one of the three modes, where the W-state is detected in. The reflected photons mode shall be denoted by b_0'. With two mirrors this mode is overlapped with a_0 at the overlap beam splitter BS_1. The two mirrors allow the alignment of the overlap without the need to change the coupler I_{b_0}, which would result in a different splitting ratio of the adj. BS (5.2.2.3). Only the output of BS_1 where a_0 is transmitted is used for the W-state preparation. In the other output mode the photons are detected in D_{dip} This detector just serves for the measurement of the Hong-Ou-Mandel dip (5.4), which is important for the alignment (5.5). In principle, this output could serve to prepare the W-state as well. Fig. 5.1 differs from the real setup in the setting of D_{dip} to keep a better overview. In the real setup all of the detectors have the equal distances of 55 cm to I_{a_0}, respectively I_{b_0} and therefore also to the crystal. This guarantees coincident detections[1] and equal coupling efficiencies. The mode a_0 is then split up at BS_2, where the transmission mode is called b and the reflection mode a. The photons in the experimental data will be denominated in the order a, b, c. In b the photons are analyzed directly, while in a a $\lambda/2$ plate, that is not part of the state analysis, is necessary to compensate the phase shift of π between horizontal and vertical polarization, that occurs in the reflected output of BS_2. In the modes, where the W-state is prepared (a, b and c) the polarization has to be analyzed. This is done by a $\lambda/4$ and a $\lambda/2$ waveplate followed by a PBS. D_i^H detects horizontal polarization in the transmitted output and D_i^V vertical polarization in the reflected output (where $i \in \{a,b,c\}$). For the detection the photons are coupled into fibers connected to pigtailed avalanche photo diodes. A coincidence logic (not shown in fig 5.1) registers simultaneously the signals from the eight detectors (there are 256 possible events). This data is then stored by a computer.

---

[1]With a coincidence window of the coincidence logic of 10 ns this is not crucial, however.

5.2   Description

5.2.1   The Source

As explained in the theory part spontaneous parametric down conversion (SPDC) is the source of choice for the creation of pairs of entangled photons. In the experiment pairs are generated by a short pulse of ultraviolet light. With a lower probability even two pairs are created from a single pump pulse. With increasing pump power this probability is raised. Since there is no source directly generating intense UV-pulses, an intermediate step is chosen. A Ti:Saphire-laser emits pulses of 130 fs pulse width at 780 nm with a repetition rate of 82 MHz. Via second harmonic generation in a LBO-crystal ($LiBO_4$) UV-pulses at a wavelength of 390 nm and of about 800 mW average power are generated. These UV-pulses pump a 2 mm thick BBO-crystal ($\beta BaBO_4$) to create polarization entangled photon pairs emitted under an angle of 3° with respect to the pump beam direction. Long-pass filters serve to cut off scattered light from the UV-pulses. In addition, interference filters of 3 nm bandwidth determine the spectral width of the down conversion photons. Finally the photons are coupled into single mode fibers.

5.2.2   Optical Components

5.2.2.1   The Fibers

The single mode fibers define the modes of the collected photons and guide them to the W-setup. The birefringence of the fibers change the polarization of the photons. Polarization controllers compensate this transformation. While the fiber in mode a_0 is set to output the initial polarization, the one defining mode b_0 turns the polarization by 90°. The reason for this is, that it enables us to measure the HOM-dip (5.4), which is an important help for the alignment, as explained later on (5.4). The photons are detected in fiber pigtailed avalanche photo diodes.

It is convenient to have the possibility of using single mode fibers to select well-defined modes and guarantee spatial coherence. Thus, it was important to find out, whether the coupling efficiency to single mode fibers is worse, than to multi mode fibers. To avoid loss when coupling to these fibers also the dependence of the coupling efficiency on the distance between the couplers was studied.

A 785 nm laser diode was coupled into a single mode fiber (F3224[2]), as it is used in the latter setup to collect the SPDC emission. After a certain distance varying between 18 cm and 100 cm the light from that fiber was coupled into a multi mode fiber (AS S50/125Y[2]) and also into different single mode fibers (F3224[2] and F4224[2]). For each distance the focus was aligned and the coupling efficiency tested. The outcoupling of the first single mode fiber was done with a homemade

---

[2]Thorlabs

construction, (5.2.2.2), as it will be used in I_{a_0}, offering the possibility to adjust the focal length. In fig. 5.2 the dependence on the distance of the couplers for all three fibers is shown. The coupling efficiency into the multi mode fiber is $\sim 88\%$, for the
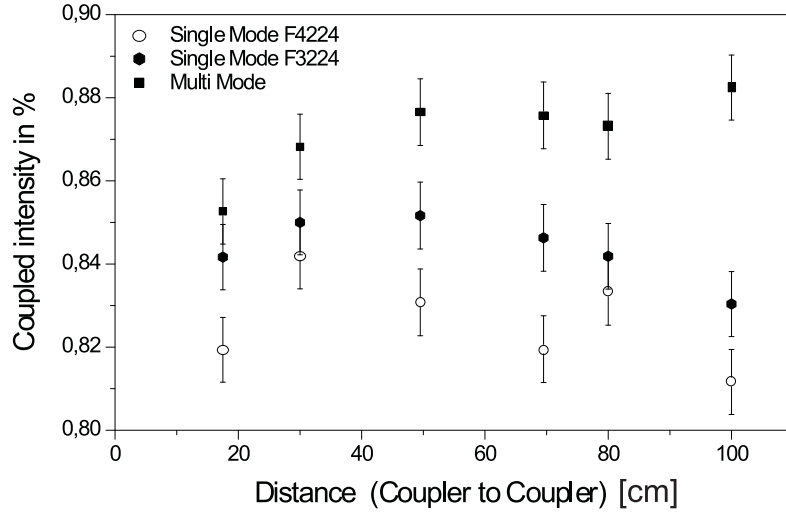

Figure 5.2: Dependence of the coupling efficiency for different single mode fibers (F3224, F4224) and a multi mode fiber (AS S50/125Y) the distance

single mode fiber F3224 $\sim 85\%$, and for F4224 $\sim 83\%$. So, the losses when using a single mode fiber are not much higher than that of the multi mode fiber. The adjustment, though, is much more difficult. A second result is, that the efficiency of the coupling is dropping for between 30 cm and 18 cm distance of $\sim 2\%$ for all the fibers. This is due to the fact, that the beam has to be focused such, that the diameter gets bigger than the lens for the incoupling. For longer distances coupling to the multi mode fiber doesn't show a dependence on the distance for the tested range. The single mode fibers, however, loose both $\sim 3\%$ in coupling efficiency between 30 cm and 100 cm. The errors have been deduced from a test of how much the coupling efficiencies vary when the fiber is unplugged, plugged and aligned again.

5.2.2.2 Fiber Couplers

In the experimental setup three different kinds of fiber couplers are used. The coupling of the down conversion emission is realized with a coupling system[3]. The coupling system allows the accurate alignment to the mode and a transversal positioning of the coupler-lens system. The distance of the same lens (f=11 mm) to the coupler is very accurately adjustable to allow an alignment of the beam focus. For

---

[3]Thorlabs

this reason the system was also used at I_{b0}. The accurate alignment of the focus is necessary for a good overlap at BS_1.

In I_{a0} a homemade fiber coupler is used. In this coupler the distance between the lens and the fiber connector can be adjusted by screwing the lens into or out of a cylinder where the fiber is connected to. With this coupler the focus can be adjusted by screwing a lens (f=11 mm) into a cylinder with a fiber connector fixed to the other end. This allows an adjustment of the focusing, which is, however, not possible without misalignment of the beam direction. Therefore this coupler was only used in a_0 and not changed anymore, after alignment.

For the coupling of the photons (respectively the alignment beam) it was enough to use a simpler version of fiber coupler, were the lens (f=11 mm) has a fixed distance to the fiber connector.

5.2.2.3   The Adjustable Beam Splitter

The photons in mode b_0 are split up at an adjustable beam splitter (adj. BS). It is adjustable in the sense, that one obtains different splitting ratios for different angles of incidence. These splitting ratios are also polarization dependent. As a preparation for the further setup the dependence on the angle of incidence was tested. As equation 4.18 shows, it is not necessary to really have a beam splitter transmitting $|H\rangle$ with probability 2/3 and $|V\rangle$ with probability 1/3 . This is just the most plausible case when looking at the schematic setup. Yet the splitting ratio rather needs to fulfill the condition deduced in the calculation of the setup (4.18, page 41):

$$\frac{\text{Transmission}_H \cdot \text{Reflection}_V}{\text{Reflection}_H \cdot \text{Transmission}_V} = \left(\frac{t_H \cdot r_V}{r_H \cdot t_V}\right)^2 = 4 \qquad (5.1)$$

where t_H, t_V, r_H, r_H are the amplitudes for transmission and reflection of H- and V-polarization as used in 4.4. As we will see, this condition (in contrast to the 1/3:2/3 splitting ratio) can be fulfilled exactly by the adj.BS, which was bought from EKSMA with the following specifications:

material	BK7
size	25,4 × 3 mm
flatness	$\lambda/10$ @ 633 nm
T_H/T_V	66/33($\pm$3) %
angle of incidence	45°

To find the angle where the beam splitter provides the ratio of (5.1) and to test for possible birefringence the beam splitter was characterized for angles of incidence between 40° and 55° (fig. 5.3).

A $\lambda/4$ and a $\lambda/2$ wave plate prepare the polarization out of a laser diode running on 785nm before a fiber to be horizontal at the output of the fiber. Another PBS
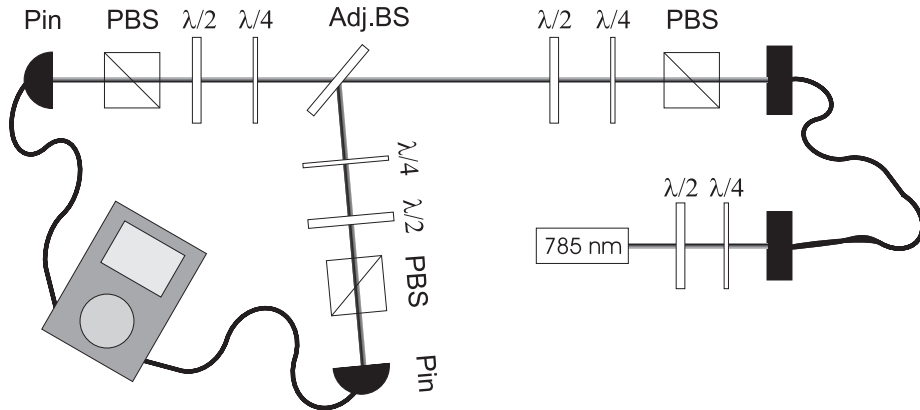
Figure 5.3: Setup to characterize the adj. beam splitter:

ensures the that the polarization is exactly horizontal. The next λ-plates are meant to prepare any polarization. The adj. beam splitter is mounted onto a rotation stage with a 2° scale.

The first test was done by measuring the intensity of both output arms for horizontally and vertically polarized beams.

Figure 5.4 shows the normalized transmission and reflection coefficients for both H- and V-polarization (T_H, R_V and T_V, R_H) in dependence of the angle setting of the adj. BS. The data was interpolated by a second order polynomial fit. Because there is no angle, where $T_H=R_V=1/3$ (neither $T_V=R_H=2/3$) the adj. BS doesn't allow to use this plausible solution (4.3) as setting. Fig. 5.5, however shows that condition (5.1) is fulfilled for an angle of 46.1°. Around this angle the ratio varies about 0.5 % per degree.

The second test analyzes the polarization behind the adj. BS (5.3) for unwanted birefringence. In each output a $\lambda/4$ and a $\lambda/2$ waveplate transform the polarization to vertical, which results in minimal transmission through the PBS. By backward calculation the information about the polarization behind the adj. beam splitter is obtained. The following table summarizes the results of the polarization analysis in the reflected and transmitted output for different input polarization at the incident angle of 46.1°:
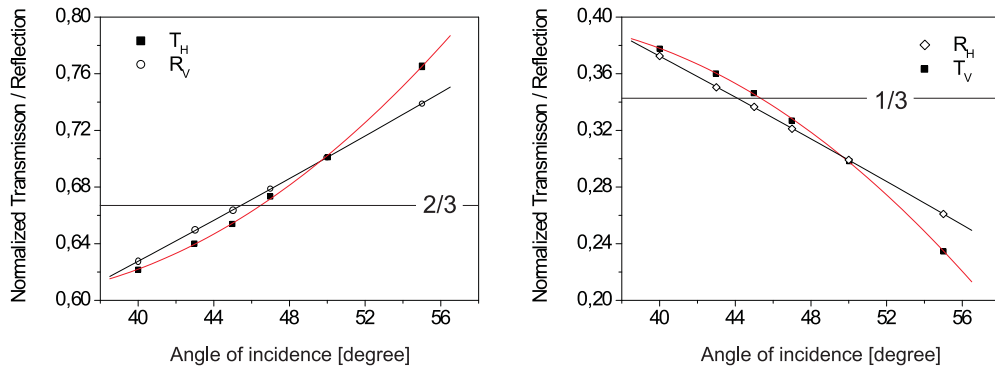
Figure 5.4: The dependence of the transmission and reflection coefficients on the angle of incidence
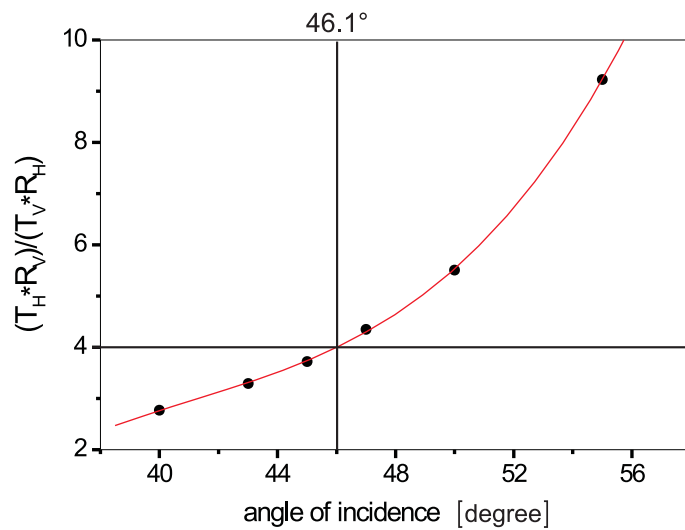
Figure 5.5: The decisive ratio for the setting of the adjustable beam splitter

Polarization	Vector	Transmitted	Reflected
H	$\begin{pmatrix} 1 \\ 0 \end{pmatrix}$	$\begin{pmatrix} 0.999 \\ 0.044e^{i0,063\pi} \end{pmatrix}$	$\begin{pmatrix} 0.999 \\ 0.037e^{i0,25\pi} \end{pmatrix}$
V	$\begin{pmatrix} 0 \\ 1 \end{pmatrix}$	$\begin{pmatrix} 0 \\ 1 \end{pmatrix}$	$\begin{pmatrix} 0 \\ 1 \end{pmatrix}$
+	$\begin{pmatrix} \frac{1}{\sqrt{2}} \\ \frac{1}{\sqrt{2}} \end{pmatrix}$	$\begin{pmatrix} 0.814 \\ i\,0.581e^{-i0.010\pi} \end{pmatrix}$	$\begin{pmatrix} 0.566 \\ i\,0.825e^{+i0.035\pi} \end{pmatrix}$
-	$\begin{pmatrix} \frac{1}{\sqrt{2}} \\ -\frac{1}{\sqrt{2}} \end{pmatrix}$	$\begin{pmatrix} 0.814 \\ i\,0.581e^{-i0.006\pi} \end{pmatrix}$	$\begin{pmatrix} 0.585 \\ -i\,0.811e^{+i0.028\pi} \end{pmatrix}$

The input polarization is shown in the first column with the corresponding vector in the second one. In the third and fourth column the vectors represent the polarizations in the outputs. They are normalized and the multiplication with a global phase makes the phases in the vector appear in the second component of the vectors. The coefficients are close to the expected ones (given by $r_H = t_V = \frac{1}{\sqrt{3}} \approx 0.58$ and $r_V = t_H = \frac{1}{\sqrt{3}} \approx 0.82$). We are more interested in the phase shift between H- and V-polarization. The vectors are written such, that the phases appearing in the exponent are those, caused by birefringence. The error in the phase caused by the setting of the wave plates (about 0.5° is the estimated insecurity) causes $\sim \pm 0.015$ error in the relative phase between H and V. This results in an error of $\sim \pm 0.045$ for all of the three wave plates. When looking at the phases shown in the table above, they are found to be inside the range of error. The error in the coefficients is about $\sim \pm 0.06$. This means, that the birefringence of the adj. beam splitter is negligible and does not need compensation.

5.2.2.4   Beam Splitters

The symmetric beam splitters[4] were tested in a similar setup as the adj. BS, to check the splitting ratio and the absorption. In this test it was found, that it is possible to vary the splitting ratio for vertical polarization, by a rotation around the vertical axis. The effect on the horizontal polarization splitting was negligible and therefore not to align. In the end the absorption was found to be $\sim 1\%$ and splitting ratio for

---

[4]Newport

horizontal polarization of T_H:R_H $\sim$ 51:49 could be achieved. The one for vertical polarization can in principle be set to be fully symmetric.

The polarizing beam splitters[5] are known to reflect some unwanted horizontal polarization, while they almost don't transmit vertical polarization. By turning the PBS around its vertical axis it is possible to decrease the error in the reflected arm. On a screen one can observe a spot of the reflected beam for an incident horizontal polarization. Because 780 nm wavelength is near infrared the spot not visible. A CCD-camera was used to show the spot on a monitor. The PBS is rotated to the position where the spot shows the least brightness. A test with PIN-Diodes showed, that instead of $\sim 1\%$ (for alignment by back reflection) only $\sim 0.2\%$ horizontally polarized light was found in the reflected arm. One could observe a slight degradation in the transmitted output: the transmission of V-polarized light increased from $\sim 0\%$ to $\sim 0.2\%$. The PBS for the state analysis were aligned this way. PBS_{trig} is an important part of the state preparation. For this reason another type of PBS[6] was used here offering an error $< 0.1\%$ in transmission and $\sim 0.5\%$ in the reflected arm.

5.2.3   The detection

The single photon detectors are fiber pig tailed silicium avalanche photo diodes (APD[7]). These multi mode fibers are connected to fiber couplers F220FC (5.2.2.2). For the construction there was usually an additional single mode fiber between the coupler and the multi mode fiber. For the detection of single photons the APD's are used in Geiger Mode. When an avalanche is triggered by a photon a current starts to flow and is detected by a proper electronics. The diodes are quenched to avoid damage. The detection of up to eight photons (that is 256 possible events) is computes by a fast coincidence logic and stored by a computer.

5.3   Construction

This section describes the stepwise construction of the W-state preparation setup. An alignment beam is necessary for the first few steps of the procedure. Thus, a part of the pulsed light from the Ti:Sa-laser was coupled to a symmetric fiber beam splitter. To cause no misalignment when plugging and unplugging, the fibers in modes a_0 and b_0 were assembled out of two two meters parts with one part fixed to the couplers I_{a0} or I_{b0}. They could be connected to the fiber beam splitter for the construction and afterwards to the fibers from the down conversion source.

---

[5]Laseroptik
[6]Newport
[7]Perkin/Elmer C309025QC-02

5.3.1 The First Path

The crucial part of the experiment is the interference of the two photons at beam splitter BS_1. Therefore the modes a_0 and b_0 have to overlap (spatial coherence) and the difference in the path lengths has to be zero (temporal coherence). To control the delay in one arm the fiber coupler I_{a_0} is mounted onto a translation stage moving in the direction of a_0. There are two important conditions on the outcoupling at a_0: Firstly, the mode of the beam needs to be independent of the position of the translation stage, so that the overlap stays the same when the translation stage is moving. Secondly, the coupling efficiency from I_{a_0} to the detectors needs to be optimized and also to be independent from the position of the translation stage.

So the direction of the beam was aligned to be parallel to the movement of the translation stage and a fiber coupler was set in a distance of $55\,\mathrm{cm}$ from I_a (this will be the distance to the detectors in the final setup) to check the alignment and the coupling efficiency. The focus of the beam was adjusted with the homemade coupler described before to optimize the coupling efficiency to the fiber. The dependence of the coupled intensity from the movement of the translation stage was tested. This is also a very accurate test for the stability of the mode, because slight changes already result in a deterioration of the coupling efficiency to the single mode fiber. After the adjustment no further realignment was necessary. The measurement in fig. 5.9 was done after the overlap was aligned and shows the coupled intensity to a single mode fiber. Over the range of $20\,\mathrm{mm}$ smooth variations of the coupled intensity of about $8\,\%$ were found. This doesn't affect the measurements, because they are performed in ranges of the order of magnitude of the region where the pulses interfere (or the photons later on), which is few hundred micrometers. The variation of $8\,\%$, however, happens over a region of $10\,\mathrm{mm}$can. It can be attributed to the imperfections of the translation stage.
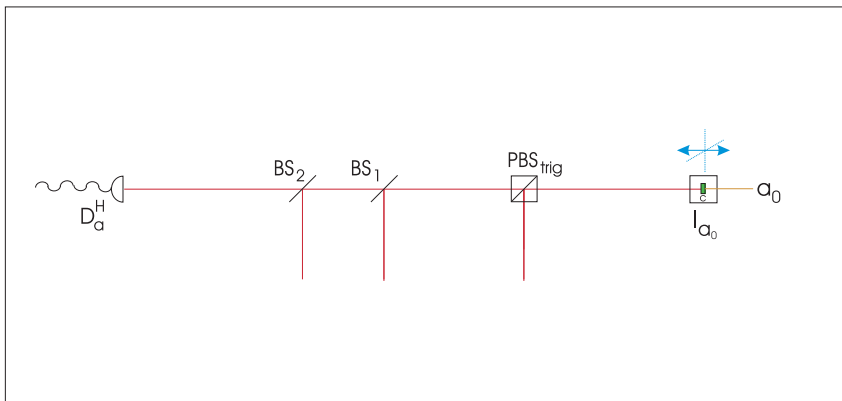
Figure 5.6: The optical components mounted and aligned after step 1

Now the mode is fixed and the beam splitters can be mounted. Their alignment is described in 5.2.2.4. Finally the detector D_2^H is aligned to the beam, with a single mode fiber at the coupler.

5.3.2   The Second Path

The fiber coupler I_{b0} is set to be parallel to the one in a_0 (see fig. 5.7). When I_{b0} is set up it is important that the position of zero delay is in the range of the translation stage. Directly after I_{b0} the adj. beam splitter is set up.

Out of the preliminary test on the adj. BS the angle of incidence needed for the right splitting ratio is known. But it is not possible to set the angle with high accuracy using the scale on the rotation stage. PIN-diodes in the output of the adj. BS were used to check the splitting ratio for fine adjustment.
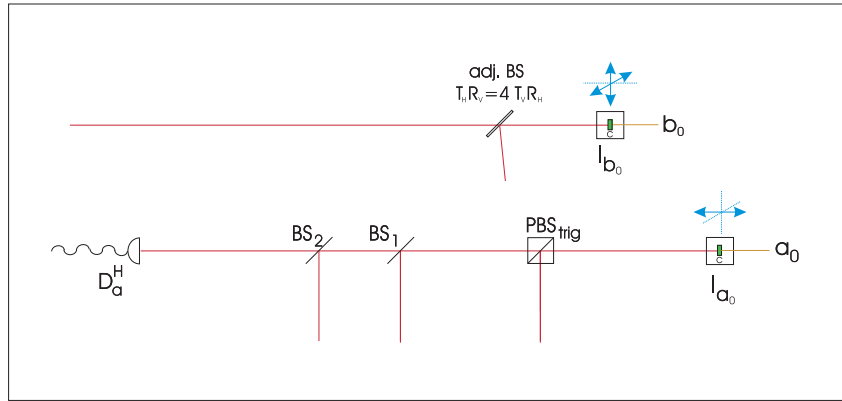
Figure 5.7: The adj.BS has to be mounted in b_0. It is aligned exactly to the right splitting ratio.

5.3.3   The Overlap

To overlap mode b_0' and a_0 at BS_1 we take advantage of the fact, that a single mode fiber is already aligned to mode a_0. The two mirrors M_1 and M_2 were set up and aligned for an optimal coupling of b_0' to the same single mode fiber. This included also an alignment of the focus in b_0. When a good coupling is accomplished, one can be sure of a fairly well aligned overlap. The overlap was also checked by looking at the other output mode of BS_1.

Up to that point there was no interference, because there was no temporal overlap of the pulses, yet. To find the position of zero delay, the translation stage was moved in steps of $10\,\mu$m to scan for interference. Strong fluctuations in the intensity appear when pulses overlap. The single mode fiber in detector D_b^H selects a single mode and guarantees the spatial coherence. The polarizing beam splitter
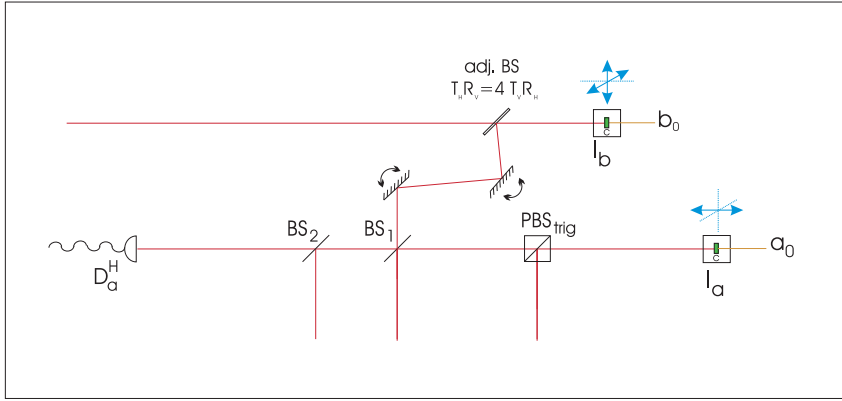
Figure 5.8: The mirrors to adjust the overlap were setup. There is only the state-detection missing.

PBS$_b$ guarantees equal polarizations. To achieve a high contrast in the interference pattern is necessary to take care, that equal intensities from a$_0$ and b$_0$ are coupled to the single mode fiber. The scan for the interference was controlled by a computer driving the translation stage and saving the positions and the intensity read out from a PIN diode that was connected to the fiber. Fig. 5.9 shows, that there are indeed strong fluctuations around the position -5.5 mm. The small graph in the same figure shows a scan in the region of interference. Because it is not possible to drive the motor in smaller steps than the wavelength, the data points seem to be distributed randomly inside the envelope of the interference. The lowest intensity is found at position -5.47 mm and is close to zero. Thus the contrast is almost 100 %. At this position the interference pattern was also checked in the other output of BS$_1$. No spatial interference fringes could be found, but slow fluctuations in the intensity due to slight changes in the optical path length. This is another hint for a good spatial overlap of the two modes.

5.3.4 Switching to Single Photons

The next step was to test the overlap with down conversion photons. First, however, a detector in the other output of the beam splitter has to be mounted to allow the detection of coincident events. Then the fibers between the W-setup and the down conversion source were connected. The polarization controllers were adjusted. To do this, a polarizer transmitting horizontal polarization is mounted before the incoupling of the down conversion emission. The output in b$_0$ is adjusted to vertical and the one in a$_0$ to horizontal polarization.

A first successful scan of a HOM-dip with a coupling into single mode fibers is shown in fig. 5.10. Before the analysis of this dip will follow in the next section I want to finish the description of the construction. After the alignment of the overlap
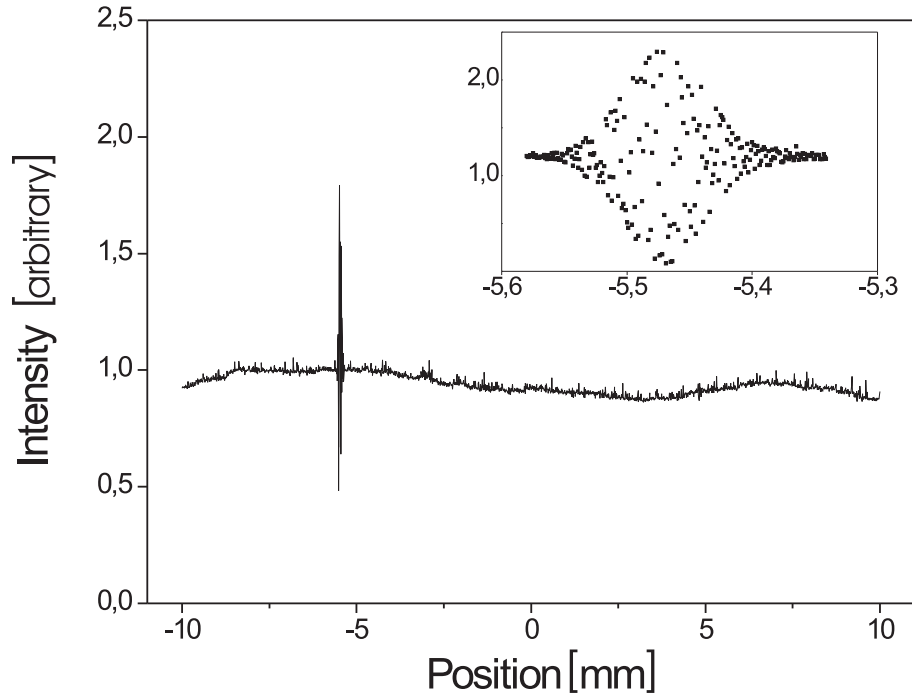
Figure 5.9: The scan for the position where the pulses overlap. The small picture shows a scan over the range where the overlap was expected. One can also see, that the coupling stays very stable over the whole range

has proofed to work with the single photons the polarization analysis for b and c, the trigger detector D_{trig} and D_a^V were mounted using the alignment beam.

5.4   The Hong-Ou-Mandel Dip

In the theory part it was already explained (4.2), that photons entering a symmetric beam splitter always leave in the same output mode if they cannot be distinguished. To achieve this it is necessary to guarantee spatial, temporal and spectral coherence. To observe the second-order interference we are using the photon-pairs created by the source.

Due to the transformation performed in fiber b_0 the state $|\psi^+\rangle$(emitted from the down conversion – section 4.1) is transformed to:

$$|\phi^+\rangle = \frac{1}{\sqrt{2}}(|HH\rangle + |VV\rangle)$$
(5.2)

PBS_{trig} doesn't allow for V-polarized photons to reach BS_1. Thus, only H-polarized photons overlap.

The Scan   To observe the HOM-dip it is necessary to change the path length of mode a_0 and register the coincidence rate between D_{dip} and D_b^H (N_{dip}). For this experiment it is even more interesting to look at the coincidence rate between detectors D_b^H and D_a^H (N_{bump}), because for the W-state the events where the photons enter the same mode are selected. N_{bump} should show a bump for zero delay with twice the count rates compared to the rates outside the region of interference. The scan was controlled by a computer driving the translation stage and storing the positions and count rates.

Evaluation   To evaluate the scan we use a theoretical dependence of the coincidence count rate from the path delay.

We assume our filters to have a gaussian spectral distribution. Therefore the coherence time is given by the inverse of the bandwidth:

$$\Delta\tau \simeq \frac{1}{\Delta\omega} \tag{5.3}$$

Further we assume that BS_1 is perfectly symmetric. Out of the expression 4.16 (page 35) we can deduce:

$$N_{dip} = C\left(1 - e^{-\frac{\Delta t}{t_c}}\right) = C\left(1 - e^{-\frac{\Delta x}{l_c}}\right) \tag{5.4}$$

where Δt is the temporal and Δx the spatial delay in the paths.

C is the coincidence count rate outside the dip and t_c and l_c are the coherence time and length.

Experimentally, the count rates for the coincidence dip do not go down to zero. The visibility is defined as:

$$V_{dip} = (N_{dip}^{max} - N_{dip}^{min})/N_{dip}^{max} \qquad \text{for the coincidence dip and}$$

$$V_{bump} = (N_{bump}^{max} - N_{bump}^{min})/N_{bump}^{min} \qquad \text{for the bump.}$$

The fit function, that is used for the evaluation of the experimental data is then:

$$y(x) = C\left(1 - Ve^{-2\left(\frac{x-x_0}{l_{dip}}\right)^2}\right) \tag{5.5}$$

C: The count rate in the classical regime

V: The visibility as defined before (with a negative sign for a bump)

x_0: The position of the minimum (maximum) value of the dip (bump)

l_{dip}: 2σ-width of the gaussian curve.
By comparison with the theoretical prediction (5.4) we conclude, that the resulting coherence length is $l_c = \sqrt{2}l_{dip}$.
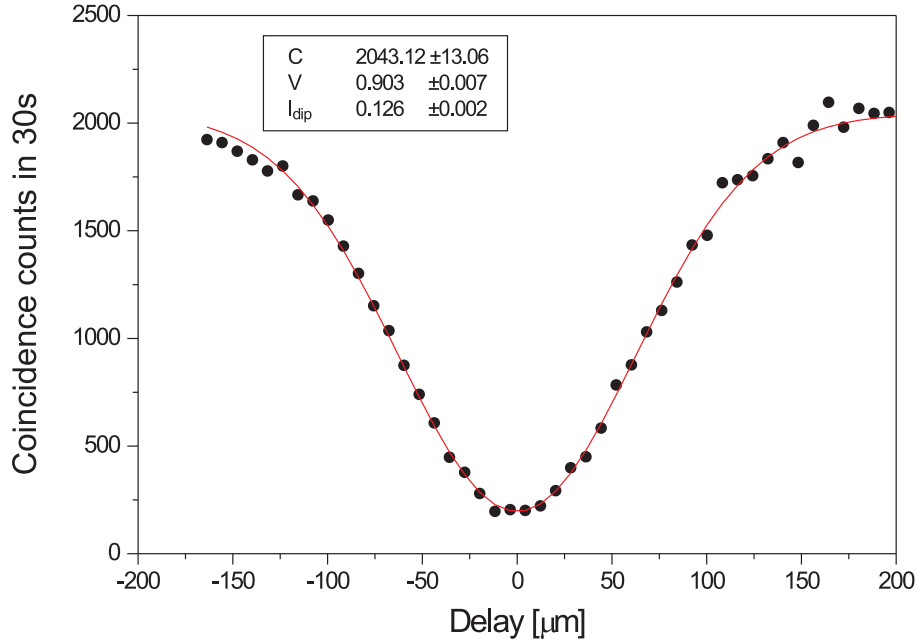
Figure 5.10: A HOM-dip measured with single mode fibers at the detectors for mode selection.

Measurements Two interference scans are included in this analysis:

First, a coincidence dip, where both of the photons were coupled into single mode fibers. It was observed directly after the overlap had been built up (fig. 5.10).

Second, a measurement, that is representing the measurements performed for the alignment of the setup. The photons were coupled directly into the multi mode fibers of the detectors. A coincidence bump (in the count rates N_{aH-bH}) and two coincidence dips (in N_{aH-dip} and N_{bH-dip}) are included (5.11).

Single Mode Dip Fig. 5.10 shows a visibility $V_{dip} = 90.3 \pm 0.7\%$. Theoretically it is possible to reach a visibility of 100%. Single mode fibers select the mode, thus the spatial coherence of the detected photons can be assumed to be perfect. Therefore we can expect to have this visibility as an upper bound when aligning the spatial overlap with the multi mode fibers. Another factor is the splitting ratio of the beam splitter BS_1. As one can see in 4.2 the visibility is reduced by a factor:

$$\frac{2RT}{R^2 + T^2} < 1\% \tag{5.6}$$

for $T : R \approx 51 : 49$, with the error found in the test of the beam splitter (5.2.2.4). Therefore, this is also negligible. Further possible reasons are the spectral coherence, and random coincidences (coincident detection of photons that were not created as a pair). Errors occur, when a pair of photons is not equally polarized due to the source or due to imperfections in the polarization alignment of the fibers.
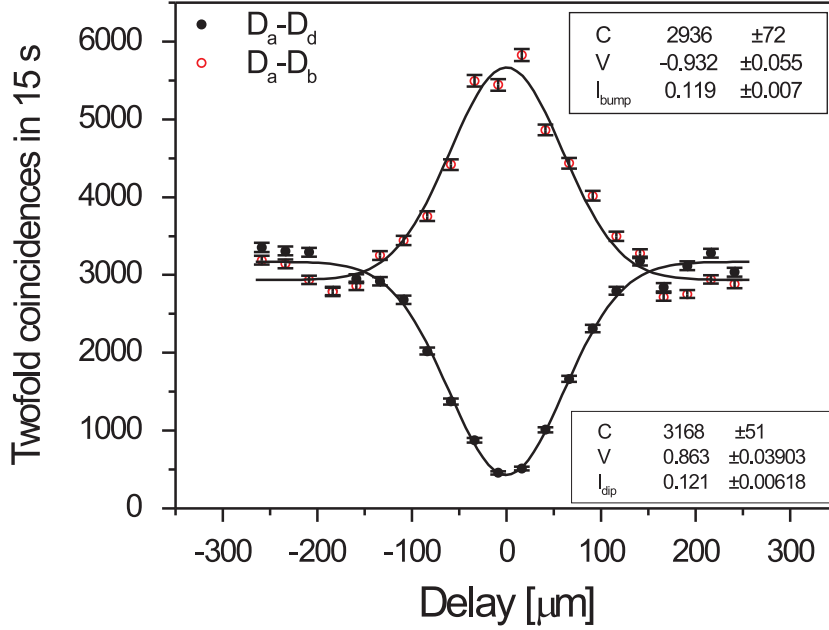
Figure 5.11: Coincidence dip (D_a^H,D_{dip}, full circles) and bump (D_a^H,D_b^H, open circles). The maximum interference occurs at zero delay between the photons arriving at BS_1. The risibilities are $V_{dip} = 86.4 \pm 0.4$ and $V_{bump} = 93.3 \pm 0.6$

Multi Photon Dip   The coincidence dip in fig. 5.11 shows a lower visibility than the one into single mode fibers: $V_{dip} = 86.4 \pm 0.4 \, \mu m$. It is lower, because there is no mode selection from the fibers. A non-perfect overlap of the modes is responsible for the degradation of the visibility. The width of the gaussian fit is $l_{dip} = 122 \pm 1 \mu m$ and is in the same order of magnitude as the one shown before. The count rates outside the dip are now around 3200 per 15 sec.

In figure (5.11) one can also see the coincidence bump between the detectors D_a^H and D_b^H of the same measurement. The width is similar to the one of the dip ($l_{bump} = 119 \pm 7 \mu m$). The visibility, however is higher than the one observed in the dip ($V_{bump} = 93.3 \pm 5.6 \, \mu m$).

5.5   Alignment

The count rates of four-fold coincidences in the experiment were to low to allow the alignment of the setup directly by optimizing the signal of the W-state itself. It was necessary to have criteria about the quality of the alignment out of the two-fold coincidence count rates. This section will introduce the criteria that had to be fulfilled to expect a good measurement and how they were applied for the alignment. A mathematica program was used to extract the events of interest out of the 256 events that were stored for each time interval of the measurement. In short test

runs of a few seconds one could extract the necessary information.

Count Rates   Before any further alignment the coupling to the detector fibers is checked. Therefore the fiber couplers for the collection of the conversion photons are adjusted for maximum single (S) and two-fold coincidence (C_2) count rates. This is done online, with a computer program displaying the current count rates. In a test run it is possible to check the ratio S:C_2. If this ratio reaches values of about 0.04 (with $6000\,C_2/h$) one can expect the four-fold coincidence count rate to reach about $70\,counts/h$.

Polarization Alignment   The polarization compensation in the fiber was already aligned in the initial alignment of the setup. It turned out, however, that this alignment was not enough. Especially, a good adjustment at PBS_{trig} is crucial, because it is responsible for the filtering of the four-photon processes with equal polarizations in each mode. These contributions are together twice as probable as the ones that properly contribute to the W-state. This can be seen in equation 4.8 on page 33. In the first measurement of the W-state this led to high contributions of unwanted terms. When looking at the two-fold coincidences one can see, that a wrong polarization alignment in a_0 results in an increase of coincidence counts between detector D_c^H and D_{trig} ($N_{cH-trig}$) which should only detect V-polarized photons. This event has high count rates and therefore is useful for an online alignment. To use it as a reference, it is preferable to minimize at the ratio of $N_{cH-trig}$ to $N_{cV-trig}$. After optimization typical values were:

$$\frac{N_{cH-trig}}{N_{cV-trig}} = 2\,\% \tag{5.7}$$

This value enters linearly in the contribution of unwanted $|HHH\rangle$ events to the W-state.

HOM-Dip   A good aligned overlap is crucial for the preparation of the W-state. Thus a new alignment of the overlap is necessary before each measurement. The mirrors M_1 and M_2 are adjusted, while the translation stage is at the position of maximum interference. For a good overlap one tries to minimize the dip count rates. To ensure, that bad coupling is not the reason for a decreasing count rate the bump count rates are checked simultaneously. One problem in that procedure is, that an adjustment of the mirrors slightly changes the path length in b_0'. Therefore it was necessary to check the position again after some alignment and to iteratively improve the visibility. It turned out, that changes in the position on the scale of a few micrometers were occuring typically in the first times, when bigger changes were necessary. For the fine alignment, no changes could be observed anymore, and thus they were acceptable. The visibility typically reached values of about $85\,\%$ for the dip and about $90\,\%$ for the bump.

The Adjustable Beam Splitter   To test the splitting ratio of the adjustable beam splitter it is necessary to block the mode a_0. Then one can check the splitting ratio by looking at the single count events in D_a (S_a), D_b (S_b) and D_c (S_c). Usually there is a difference in the numbers of H-polarized and V-polarized photons, but optimizing for the ratio (eq. 4.18, p.41) these errors cancel. In the reflected output of the adj. BS there is now BS_1 included. Assuming that BS_1 is perfectly symmetric one needs to align the adj. BS to:

$$\frac{(S_a^V + S_b^V) \cdot S_c^H}{(S_a^H + S_b^H) \cdot S_c^V} = 4 \tag{5.8}$$

This was achieved up to an error of $0.5\,\%$. It turned out, that once the adj. BS is set to the correct ratio, no realignment is necessary.

6 Analysis of the State

In this chapter, I present the results, that have been obtained with the W-state setup so far. But first, some remarks on how the data were analyzed will be necessary. The first measurement presented is a zzz-basis measurement as this was also the first measurement performed with the setup. Then a xxx-basis measurement will follow to test, whether the state is fulfilling the theoretical predictions also for another basis.

6.1 Data Preparation

The count rates of interest are extracted from the 256 events registered by the coincidence logic via a mathematica program. The relative efficiencies of the detectors have been measured independently. The efficiency of a four-fold coincidence is calculated by the product of the efficiencies of the participating detectors. Then the raw count rates are corrected for the efficiencies. That are the data presented here.

Two sources of errors contribute to the overall error on the statistics shown: Firstly, the fluctuations in the count rates due to Poissonian statistics ($\Delta N = \sqrt{N}$) and secondly the errors in the measured efficiencies. In this analysis, I will consider three fold coincidences, because the trigger photon doesn't contribute to the state – though all four-photons are necessary. events.

6.2 Population in xxx and zzz

6.2.1 zzz-Basis

The first measurements, performed after the built-up and alignment was ready, were done in the zzz-Basis (A.1).

In a zzz-basis measurement, one analyzes every photon for $\{|H\rangle, |V\rangle\}$ and where the wave-plates in every polarization analyzer (for a,b and c) are set to $0°$.

The data shown here were collected over 10 hours. A total number of 1439 counts was found for the W-state. One clearly observes contributions from the W-state product terms HHV, HVH and VHH. The background of other contributions is 113 ± 26 counts which corresponds to $7.9 \pm 1.9\%$
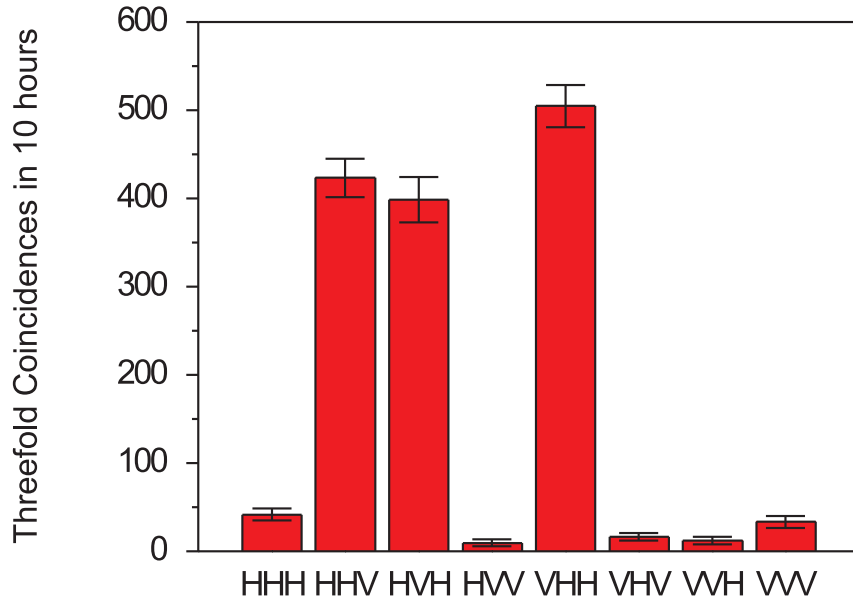
Figure 6.1: Three-fold coincidences in 10 hours of a zzz-measurement, i. e. with horizontal/vertical polarizer settings

Reasons for the background are compensation of the birefringence in the fiber and non-perfect correlations in the state produced by the source. The main contribution, however, is the imperfect filtering of 4-photon events with equal polarizations in each mode by PBS_{trig} resulting in the HHH and VVV term.

HHV	$29.4 \pm 2.1\%$
HVH	$27.7 \pm 2.0\%$
VHH	$35.1 \pm 2.4\%$

The VHH contribution is higher than the other two. So the ratio between these events still has to be improved.

The correlation of the measured state is calculated out of the joint probabilities:

$$C_{zzz} = P_{HHH} - P_{HHV} - P_{HVH} + P_{HVV} - P_{VHH} + P_{VHV} + P_{VVH} - P_{VVV} =$$
$$(N_{HHH} - N_{HHV} - N_{HVH} + N_{HVV} - N_{VHH} + N_{VHV} + N_{VVH} - N_{VVV})/N_{tot}$$

where N_{event} is the number of counts for an event (e.g. HHH) and N_{tot} is the overall count rate. Theoretically the correlation should be equal to -100%, theoretically. Experimentally we find:

$$C_{zzz} = -88.9 \pm 3.4\% \qquad (6.1)$$

6.2.2 xxx-Basis

A measurement in the xxx-basis is realized by setting the $\lambda/2$ wave plates to 22.5° in each arm (a,b and c). For this measurement the compensation plate in the reflected output of BS_2 was missing which resulted in a detection of $(+)$ (i. e. 45°-polarization) for $|-\rangle$ and vice versa. This was corrected in the data by exchanging the role of the outputs of PBS_b. The measurement was running over a time of 3h, with a total
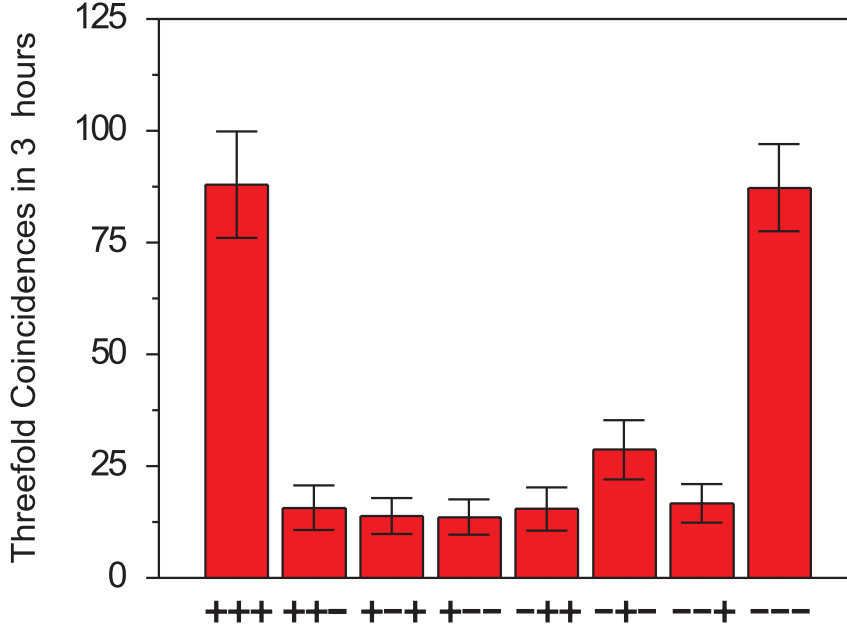
Figure 6.2: Three-fold coincidences in 3 hours of a xxx-measurement, i. e. with $\lambda/2$ wave plates at 22.5°

number of 279 counts.

According to the theory (3.2.1), we find the $(+++)$ and $(---)$ with the highest probability:

$+++$	$31.5 \pm 4.8\,\%$
$---$	$31.3 \pm 4.1\,\%$

They exceed the value of 0.25, that was predicted for ρ_{fool} by 6 %, this confirming the observation of the W-state. Both terms contribute equally and are close to reach the theoretical value of $3/8 = 37.5\,\%$ with an error of 6%.

The terms with lower counting rate are all around $\sim 5\%$, except for $(-+-)$, which contributes $10.3 \pm 2.5\,\%$. They are expected to have a probability of $1/24 \approx 4\%$ and thus most of the contributions are very close to the prediction.

The W-state is invariant under permutation of particles. The data presented in fig. 6.2 illustrates this. In theory it is expected to be zero, whereas the experimental

value obtained by analogue calculation as in the zzz-measurement is:

$$C_{xxx} = 7.7 \pm 5.3\%. \tag{6.2}$$

6.3   Two-Photon Correlation

In this section, I will analyze the experimentally prepared state for the two-particle entanglement contained therein, for example the state of the two remaining particles is depending on the measurement outcome of the third particle in the z-basis.

As it was shown in section 2.1, maximally entangled states have full correlations for measurements in more than one basis. Therefore the analysis was done by measuring the remaining two particles in both the zz-basis (i.e. H/V polarization) and in the xx-basis (+/-45° polarization). This is a procedure often used to test the entanglement, for example when the down conversion source was aligned. Theoretically (see section 3.2) one expects the correlation C to be -100 % for the measurement in the zz-basis. In the xx-basis, the correlation is +100 % (in theory) only if the measurement outcome on the third particle was H, and 0 % otherwise.

The test is performed for all three pairs of particles. Six measurements were necessary: Firstly, a zzz-measurement (test for H/V-polarization in each arm), and three measurements where only one particle is analyzed in z-direction: zxx, xzx and xxz (the order of the bases correspond to the order of the arms a,b and c where the state is detected). The measurements were performed directly one after another, and every measurement was running over 2 hours. In figure 6.3 the results are shown, where $z_a = H$ means that the statistics of the photons in b and c is conditioned on the outcome H of the measurement on the photon in a. In the same notation is used for the other possibilites. The 2-particle correlation is depicted for every graph.

Results: For z_a=H we find a correlation of $-81.2 \pm 11.2\%$ in the zz-basis for the other two photons $74.1 \pm 11.3\%$ in the xx-basis. This is in principle high enough to violate the CHSH-inequality 2.18. To violate a CHSH-inequality the correlations must exceed $1/\sqrt{2}$ of the predicted value, that is -70.7 % (+70.7 %) for the zz- (xx-)basis measurement.

The background is due to imperfect correlations in the source and the polarization alignment, which is responsible for other contributions from the four-photon state.*that*should –in principle – be filtered – see also (6.2.1).

In contrary, the correlations for the zz-basis and xx-basis are $97.4 \pm 15.9\%$, and $-2.7 \pm 14.7\%$ respectively. As expected, there is no entanglement left.

The lower background compared to the situation described prior (z_a=H) can be explained by the fact, that the unwanted four-photon terms (where all the four photons are equally polarized) contribute less. The reason is, that the HH and the VV contribution make the background in the first case. With the trigger detected

as V and the photon on which is conditioned in H, contributions like HHHV and VVVH (without respect of the order) contribute to the background, and thus only one photon of the "unwanted" terms has to be detected wrongly to make either HH-, or VV- background. The background in the case z_a=V needs contributions like HVVV, VHVV and VVVV. They are created only by erroneous contributions due to four V-polarized photons, but not from four H-polarized ones (as in the case of z_a =H).

Also for the measurement of the photons in a and c conditioned on the outcome H in b show predicted behaviour. The correlations are even stronger in the xx-basis. We find $-0.839 \pm 10.7\%$ and $0.837 \pm 10.9\%$ for the zz- and the xx-basis, respectivley. Again the correlations are higher for z_b=V, due to the reason explained before. The measurement where the residual entanglement between the photons in b and c is analyzed shows weaker correlations. Actually, the correlations in the xx-basis measurement with $C = 55.7 \pm 11.6\%$ are to weak to expect a violation the CHSH-inequality. The most probable reason is a phase shift between V and H
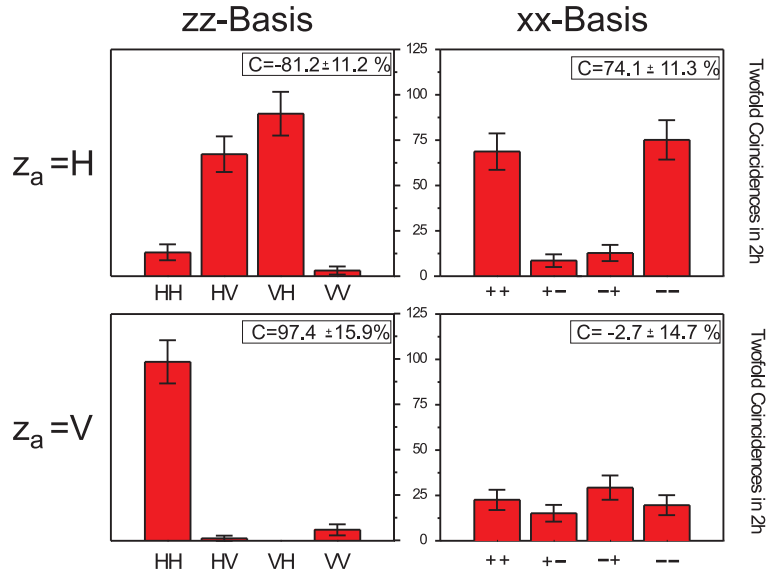
Figure 6.3: Joint probabilities for the photons b and c in dependence of the measurement outcome in a.

polarization in the overlap beam splitter, or in BS_2. This effect has been observed with beam splitters and the next step in the further development of the setup is the compensation of this phase. The phase shift effect is stronger in the measurement of the correlations between photons in a and b because both of them are effected by the phaseshift, whereas in the other two measurements only one photon of them passes these beamsplitters. In 5.2.2.3 the adj. beam splitter has been tested and showed no sign of a phase shift.

In comparison of the three measurements one can also see, that the contributions of the terms in the zz-basis by conditioning on H are equally high for the last measurement, but that HV contributes less in the first two cases. This is due to the overlap at BS_1. In an ideal case the HOM-dip and bump (see section 5.4, page 56) shows 100 % visibility and the HV and VH term have to contribute equally. In the presented setup, the bump only has a visibility of $\sim$ 90%, and therefore the contributions where H-polarized photons are overlapped, which are the mentioned contributions (HV in the zz-basis for $z_{a/b} = H$), should be lower.

In summary, one can conclude that the state observed shows entanglement for the remaining two qubits under the condition that the outcome of a measurement on the third one is H, as it is predicted for the W-state. This entanglement is strong enough to violate Bell-inequalities for two of the three possible pairs. The error on the third one will most probably be compensated by a common procedure, namely the compensation of a polarization-dependent phase shift due to the symmetric beam splitters. This will be done with a quartz plate with appropriate orientation.
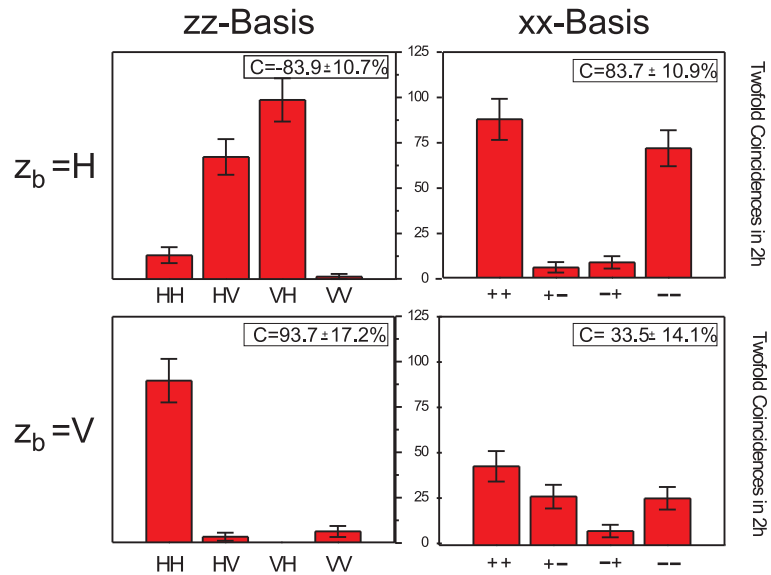
Figure 6.4: Joint probabilities for the photons a and c in dependence of the measurement outcome in b.
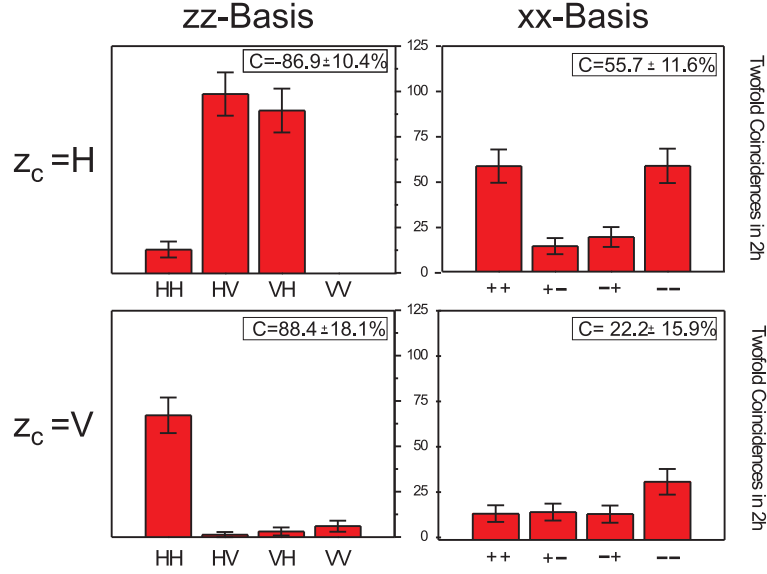
Figure 6.5: Joint probabilities for the photons a and b in dependence of the measurement outcome in c.

6.4 Correlation Functions

A correlation function was measured for the bases in b fixed to x and in c to z. This measurement is performed by setting in a rotation stage with a half wave-plate, rotating from 0° to 90°. The turn around 90° in the half wave-plate corresponds to a basis-change from z to x to z in this arm. Thus, the correlation function shows a whole periode. The measurement is performed in cicles, that is, every datapoint (angle etting) is measured for (in our case) 15 min and when all the setting were reached, it starts from the beginning. This setting corresponds to the setting xxz in the last section – this is the one where the correlations were much lower than in the other arm. Therefore it is quite natural that we will find a visibility for the correlation function that is much lower than one expects from theory, which is 66%. The correlation function is shown in fig. 6.6. We find a visibility of $32.9 \pm 5.1\%$, which is half of the expected value. To confirm the absolute orientation of the half wave plate, I introduce an additional offset angle Δ in the fitfunction in order to evaluate the visibility, which was consistent with 0. Therefore the obtained value is more accurate compared to the one in the previous section.

Again, one can use the measurement outcome of the photon in a as condition and finds 2-particle correlation functions for the remaining particle. For the outcome z_a=V the predicted correlations are 0, because the remaining state is not entangled. (The correlations in xx and xz are zero). We find a visibility of $9.6 \pm 8.0\%$. For the outcome z_a=H one theoretically finds a sine function with 100% visibility, but for the mentioned reson, that we are looking at the pair with the lowest correlations

69

we get only $48,3 \pm 10,9\,\%$, which is close to the value of $55,7 \pm 11,6\,\%$ found in the analysis of last section and, just as in the three-particle correlation about half of the expected visibility.
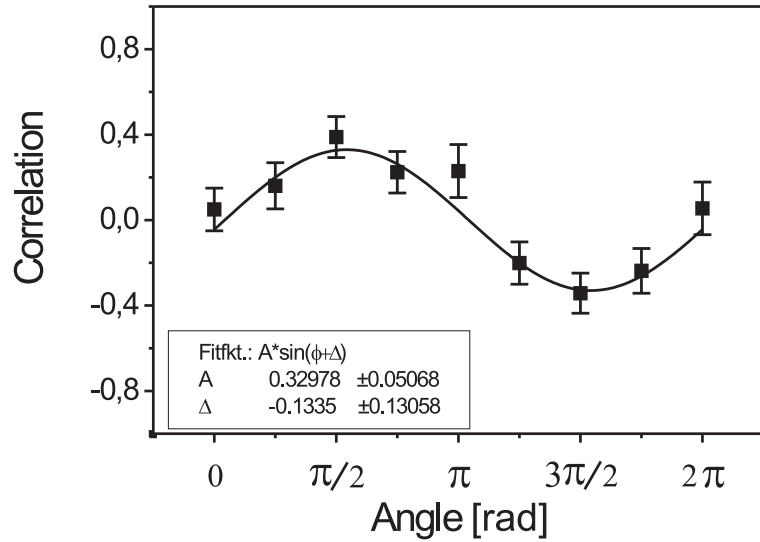

Figure 6.6: The correlation function for rotating a half wave-plate in a, with fixed bases x (+/-45°) in b and z (H/V) in c
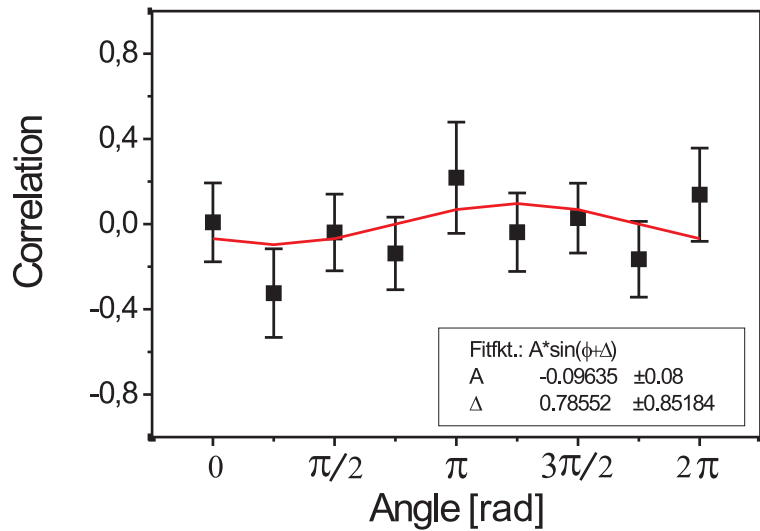

Figure 6.7: The correlation function for rotating a half wave-plate in a, with fixed basis x (+/-45°) in b conditioned on an outcome z_c=V
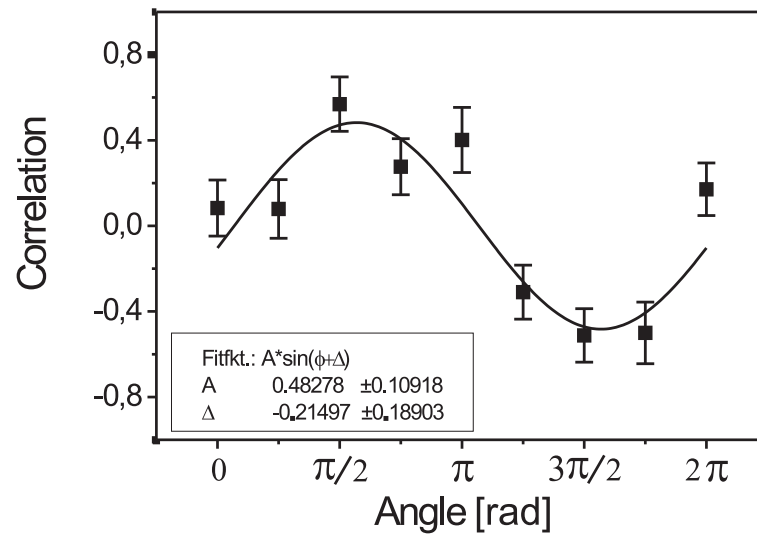
Figure 6.8: The correlation function for rotating a half wave-plate in a, with fixed basis x (+/-45°) in b conditioned on an outcome z_c=H

6.5   The Mermin Inequality

The measurements that have been used for the analysis of the two-photon entanglement between the three photons in the W-state were: zzz, zxx, xzx, xxz. This is a choice of bases that allows for a test of the Mermin inequality (section 3.3.2). The Mermin inequality for this basis-setting is:

$$-2\,\% \leq C(z,z,z) - C(z,x,x) - C(x,z,x) - C(x,x,z) \leq 2$$

Fig. 6.9 shows the three-particle joint probabilities for the four measurements with the corresponding three-particle correlation. We insert the experimentally obtained
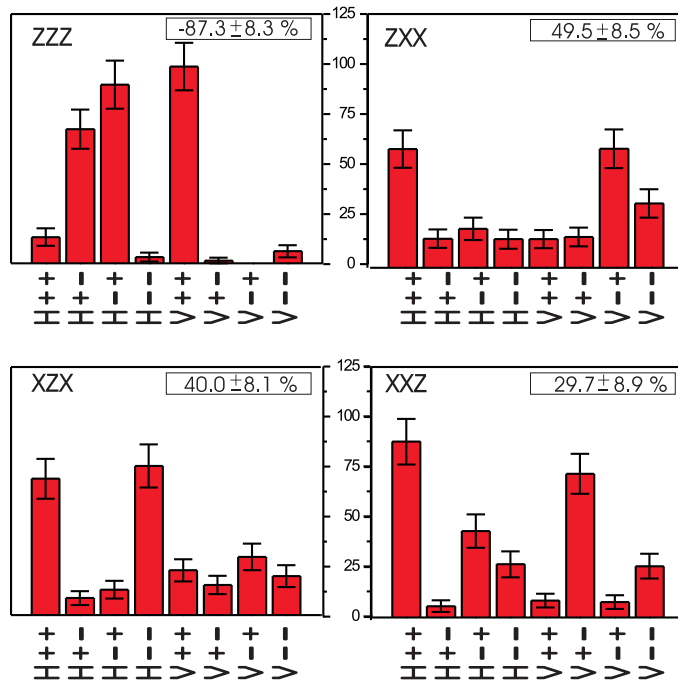
Figure 6.9: Joint probabilities in the generated state that allow for the test of the Mermin inequality

correlations (see fig. 6.9) and find for the combination of tree-particle correlation functions:

$$|-0.873\,\% - 0.495\,\% - 0.400\,\% - 0.297\,\%| = 2.065 \, > \, 2$$

Thus, the state violates the Mermin inequality by 0.065, but with an error of 0.338, therefore not in a statistically significant way. The W-state would violate this Mermin inequality with a value of 3 for that basis. However, the contribution of the xxz-basis correlation spoils this value as one already could see in the analysis of the two-photon entanglement.

7 Conclusion and Outlook

The goal of this thesis was the experimental realization of a three-photon entangled state – the W-state – and its analysis. This involved a theoretical analysis of the state and a comparison of its properties with both the GHZ-state, a state, that is known to have three-photon entanglement, and a mixed state ρ_{fool}, a state which shows for some cases a similar behavior as the W-state, but has only two-partite entanglement. The most outstanding property of the W-state is that the entanglement is mainly in the pairs, i. e. the loss or measurement of one particle does not imply the loss of all entanglement in the system.

For the experimental analysis of the state it was necessary to build an inter-ferometric setup that prepared the W-state out of the four-photon state generated by a spontaneous parametric down conversion source. The two crucial parts of this setup were the so-called adjustable beam splitter, that is responsible for the equal weighting of the terms contributing to the W-state, and the overlap of two photons on a symmetric beam splitter in such a way that the information of the mode where each photon arrived from is lost.

By a quantum mechanical calculation on the setup it was shown that the adjustable beam splitter has to fulfill certain conditions (4.18) which could be reached by the actual component. To align the overlap of the photons and to analyze its quality, pair photons generated in the first order process of the spontaneous parametric down conversion source were used. A rotation of the polarization in the fiber, that had no influence on the preparation of the W-state, allowed to interfere the initially orthogonal polarized photons. The visibilities reached with the overlap in the setup were $\sim 85\,\%$, whereas the theory predicts $100\,\%$. The visibility could be raised by the usage of interference filters with a smaller bandwidth, but this lowers the count rates in the experiment, thus, the chosen filter bandwidth of 3 nm was an acceptable compromise.

Various measurements on the generated state have been performed. A measurement of the three photons for horizontal/vertical polarization showed clearly the expected three contributions of the W-state. The background was $7.9 \pm 1.9\%$, which is mainly due to imperfections in the polarization alignment, that causes contributions that should be filtered by post-selection.

Further, entanglement between the two remaining photons after measuring one to be horizontally polarized was analyzed. This was not yet done by a Bell-inequality,

but as a first test the correlations of the photons were analyzed in the zz- and xx-basis (i. e. for horizontal/vertical and $\pm 45°$ polarization). From these correlations one can conclude that the photons were entangled, but that the entanglement was much weaker in one of the photon pairs, than in the other two, which is most likely due to a birefringence effect in the overlap beam splitter. The violation of the Mermin-inequality was not achieved due to the low correlation in the mentioned combination of photons. A measurement of the correlation function was showing a low visibility for the same reason. All together, a compensation of the phase most probably will improve the correlations for the particular setting and allow more precise measurements on the W-state.

From the correlations found in the other analyzer settings one can expect measurement results that allow for a violation of the Mermin-inequality and the inequality proposed by Adán Cabello[23]. A violation beyond Cirel'son's bound is – at least for the W-state – extremely improbable to be reached because of the small difference between the bound and a possible violation.

For further analysis of the W-state it is preferable to use the setup presented by Yamamoto et al. [37].It was proposed only very recently during the measurements on the setup used here. Because it does not involve an overlap, it is more easy to realize, more stable and promises even better correlations. It will be necessary to take care of all the birefringent phases in the beam splitters. A further interesting analysis is then a check of the entanglement robustness by performing a state tomography on two particles after the "loss" of the third one.

There are already a few possible applications proposed. There is a scheme for quantum key distribution and quantum secret sharing by J.Joo et al.[38], but that task can be most likely performed in a better way by protocols using Bell-states or the GHZ-state. Recently a quantum game was proposed by Han et al.[39] and is quite worth thinking of. A very attractive scheme deals with a so-called W-clone, a state that involves the same product terms as the W-state, but with another weighting. This state is an optimal quantum cloner and can already be realized with the presented setup by only exchanging the adj. BS with a symmetric beam splitter.

A Definitions and Notations

A.1   The Hilbertspace

There is a big variety of possible definitions and notations in the field of quantum information and foundations of quantum theory. This is mainly due to the fact that different subjects find a common playground here. To avoid confusion, I will introduce the definitions in this work shortly. The quantum mechanical system that plays the central role here is the qubit. As the experiment is using the polarization of photons, the notation is fit to this physical realization! The qubits exist in a Hilbert space H^2 with the Bloch sphere as a possible representation (see fig. A.1). Pauli-matrices are observables in this Hilbert space. Here the definitions:

$$\sigma_z = \begin{pmatrix} 1 & 0 \\ 0 & -1 \end{pmatrix} \qquad \sigma_x = \begin{pmatrix} 0 & 1 \\ 1 & 0 \end{pmatrix} \qquad \sigma_y = \begin{pmatrix} 0 & -i \\ i & 0 \end{pmatrix}$$

The eigensystems to these observables are:

$$\begin{aligned} \sigma_z|H\rangle &= |H\rangle \\ \sigma_z|V\rangle &= -|V\rangle \end{aligned} \quad \Big| \quad \begin{aligned} \sigma_x|+\rangle &= |+\rangle \\ \sigma_x|-\rangle &= -|-\rangle \end{aligned} \quad \Big| \quad \begin{aligned} \sigma_y|L\rangle &= |L\rangle \\ \sigma_y|R\rangle &= -|R\rangle \end{aligned}$$

I use z_i to denote the outcome of a measurement on qubit i in the bases defined by the basis vectors $|H\rangle$ and $|V\rangle$. Analogous for x_i and y_i:

$$z_i \epsilon \{H, V\} \ \Big| \qquad x_i \epsilon \{+, -\} \ \Big| \qquad y_i \epsilon \{L, R\}$$

It will also be necessary to talk of the eigenvalues corresponding to the eigenstates that are the basis vectors:

$$\bar{z}_i \epsilon \{+1, -1\} \ \Big| \qquad \bar{x}_i \epsilon \{+1, -1\} \ \Big| \qquad \bar{y}_i \epsilon \{+1, -1\}$$

A z-basis measurement denotes the projection onto the basis vectors $|H\rangle$ and $|V\rangle$. The definitions for x- and y-basis measurement are analogue.
If a measurement is performed on many qubits (e. g. three qubits), then a basis is chosen for every particle. Naturally, for example zxx-basis measurement is defined
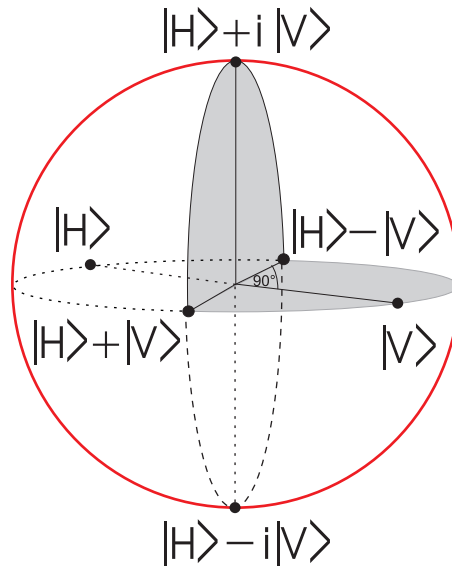
Figure A.1: Bloch-sphere representation of H^2

as a measurement where the first (in the order of the notation for the state) particle is measured in the z-basis and the other two in x.

A.2   Probabilities

At some point it is argued with probabilities. Let A an B be some events (e. g. that the particle i is measured in the z-basis and the outcome is H: z_i=H). Then

$$P(A \wedge B)$$

denotes the probability for event A *and* B. Similarly

$$P(A|B) = \frac{P(A \wedge B)}{P(A)}$$

denotes the probability for A under the condition B.
An example for the way joint probabilities are denoted is (for the zz-basis):

$$P_{++} = P(z_i = H \wedge z_j = H)$$

and $P_{+-} = P(z_i = H \wedge z_j = V)$ etc.

Bibliography

[1] D. Bouwmeester, K. Mattle, M. Eibl, H. Weinfurter, and A. Zeilinger. *Experimental quantum teleportation.* nature, **390**, 575 (1997).

[2] C.Kurtsiefer, P.Zarda, M.Halder, H.Weinfurter, P.M.Goreman, P.R.Tapster, and J.G.Rarity. *Quantum Cryptography: A step towards global key distribution.* nature, **419**, 450(2002).

[3] A.Müller, H.Zbinden, N.Gisin. *Quantum Cryptography over 23 km under lake Geneva.* Eur. Phys. Lett., **33**, 335(1996).

[4] E. Schrödinger. *The fundamental idea of wave mechanics.* http://www.nobel.se/physics/laureates/1933/schrodinger-lecture.pdf, **Nobel lecture**, (1933).

[5] E.Schrödinger. *Die gegenwärtige Situation in der Quantenmechanik.* Naturwissenschaften, **23**, 807(1935).

[6] A.Einstein, B.Podolsky and R.Rosen. *Can quantum-mechanical description of physical reality be considered complete?* Phys. Rev., **47**, 777 (1935).

[7] J.S.Bell. *On the Einstein-Podolsky-Rosen paradox.* Physics, **1**, (1964).

[8] M.A. Nielsen, and I.L.Chuang. *Quantum Computation an Quantum Information.* M. Kafatos(Kluwer Academic Dordrecht, 1989.

[9] W.Dür,G.Vidal and J.I.Cirac. *Three qubits can be entangled in two inequivalent ways.* Phys. Rev. A, **62**, 062314 (2000).

[10] D. Bouwmeester, J.-W. Pan, M. Daniell, H. Weinfurter, and A. Zeilinger. *Observation of Three-Photon Greenberger-Horne-Zeilinger Entanglement.* Phys. Rev. Lett., **82**, 1345 (1999).

[11] J.-W. Pan, D. Bouwmeester, M. Daniell, H. Weinfurter, and A. Zeilinger. *Experimental test of quatnum nonlocality in three photon Greenberger-Horne-Zeilinger entanglement.* nature, **403**, 515 (2000).

[12] J.F.Clauser, M.A.Horne, A.Shimony, R.A.Holt. *Proposed experiment to test local hidden-variable theories.* Phys. Rev. Lett., **23**, 880 (1969).

[13] D.Bohm. Quantum Theory. Prentice-Hall, Englewood Cliffs, NJ, (1951).

[14] D.M.Greenberger, M.A.Horne, A.Shimony, A.Zeilinger. *Bell's theorem without inequalities.* Am.J.Phys., **58**, 1131 (1990).

[15] Adán Cabello. *Two qubits of a W state violate Bell's inequality beyond Cirel'son's bound.* Los Alamos Archive, **0205183**, (2002).

[16] B.S. Cirel'son. *Quantum Generalizations of Bell's Inequality.* Lett. Math. Phys., **4**, 93 (1980).

[17] G.Vidal, W.Dür, and J.I.Cirac. *LOCC.* Los Alamos Archive, **0004009**, (2000).

[18] A.Acín, D.Bruß, M.Lewenstein, and A.Sanpera. *Classification of Mixed Three-Qubit States.* Phys. Rev. Lett, **87**, 040401 (2001).

[19] D.M. Greenberger, M.A. Horne, and A. Zeilinger. *Bell's Theorem, Quantum Theory and Conceptions of the Universe.* M. Kafatos(Kluwer Academic Dordrecht, 1989.

[20] M.Seevnick and J.Uffink. *Sufficient conditions for three-particle entanglement and their test in recent experiments.* Phs. Rev. A, **65**, (2001).

[21] D.F.V.James,P.G.Kwiat,W.J.Munro, and A.White. *Measurement of qubits.* Phys. Rev. A, **64**, 052312(2001).

[22] M.Horodecki, P.Horodecki,R. Horodecki. *Separability of mixed states: necessary and sufficient conditions.* Phys. Lett. A, **233**, 1(1996).

[23] Adán Cabello. *Bell's theorem with and without inequalities for the three-qubit GHZ- and W-states.* Phys. Rev. A, **65**, (2002).

[24] N.D.Mermin. *What's wrong with these elements of reality.* Physics Today, **43**, 9 (1990).

[25] N.D.Mermin. *Extreme Quantum Entanglement in a Superposition of Macroscopically Distinct States.* Phys. Rev. Lett., **65**(15), 1838 (1990).

[26] Adán Cabello. *Violation Bell's Inequality Beyond Cirel'son's Bound.* Phys. Rev. Lett., **88**, 060403(2002).

[27] N.Kiesel, M.Bourennane, C.Kurtsiefer, H.Weinfurter, D.Kaszlikowski, W.Laskowski, and M.Żukowski. *Three Photon W-State.* Accepted in Journal of Modern Optics, , (2002).

[28] Adán Cabello. *private communication.*

[29] P.G.Kwiat,K. Mattle, H.Weinfurter, and A. Zeilinger, A.V.Sergienko and Y.Shih. *New High-Intensity Source of Polarization-Entangled Photon Pairs.* Phys. Rev. Lett., **75**, 4337 (1995).

[30] H.Weinfurter and M.Żukowski. *Four-photon entaglement from down-conversion.* Phys. Rev. A, **64**, (2001).

[31] M.Oberparleiter. *Multi-Photon Statistik am Strahlteiler.* Diplomarbeit, 1989.

[32] C.K.Hong, Z.Y.Ou and L.Mandel. *Measuremet of Subpicosecond Time Intervals between Two Photons by Interference.* Phys. Rev. Lett., **59**, (1987).

[33] G.P. Guo, Y.S. Zhang. *Scheme for preparation of the W state via cavity quantum electrodynamics.* Phys. Rev. A 65, **65**, 054302 (2002).

[34] X.Wang. *Entanglement in the quantum Heisenberg XY mode.* Phys. Rev. A, **64**, 012313 (2001).

[35] X.Zou,K.Pahlke and W.Mathis. *Scheme for generation of an entangled four-photon W state.* quantph/0202090v2, (2002).

[36] Bao-Sen Shi and Akihisa Tomita. *Schemes for generating W state of paths and W state of polarization photons.* quantph/0208170v1, (2002).

[37] T.Yamamoto, K.Tamaki, M.Koashi, N.Imoto. *Polarization Entangled W State using Parametric Down-Conversion.* quantph/0208162, (2002).

[38] J.Joo, Y-J.Park, J.Lee,J.Jang. *Quantum Secure Communication with W States.* quantphy/0204003, (2002).

[39] Y. Han, Y. Zhang, G.Guo . *W state and Greenberger-Horne-Zeilinger state in quantum three-prisoner's dilemma.* Physics Letters A, **?**, (2002).

Acknowledgements

Erklärung

Hiermit erkläre ich, die vorliegende Arbeit selbständig verfasst
und nur die angegebenen Quellen und Hilfsmittel verwendet zu haben.

Nikolai Thomas Kiesel
München, den 7. Oktober 2002